N O T I C E

THIS DOCUMENT HAS BEEN REPRODUCED FROM
MICROFICHE. ALTHOUGH IT IS RECOGNIZED THAT
CERTAIN PORTIONS ARE ILLEGIBLE, IT IS BEING RELEASED
IN THE INTEREST OF MAKING AVAILABLE AS MUCH
INFORMATION AS POSSIBLE

NASA

Technical Memorandum 80678

GEOID ANOMALIES IN THE VICINITY OF SUBDUCTION ZONES

David C. McAdoo

MAY 1980

GEOID ANOMALIES IN THE VICINITY
OF SUBDUCTION ZONES

David C. McAdoo
Goddard Space Flight Center
Greenbelt, Maryland

INTRODUCTION

Lithospheric plates descend into the mantle at deep ocean trenches. This observation is a fundamental part of the theory of plate tectonics. During their descent these slabs undergo an evolution in thermodynamic state which, presumably, includes density changes. It is of prime geophysical importance to define the anomalous density structure of the slabs.

Sea-going gravimetric measurements have been used by quite a number of workers (e.g., Segawa and Tomoda, 1976; Watts and Talwani, 1975; see also Grow & Bowin, 1975) to study density structure, including that of slabs, in the vicinity of subduction zones. These studies have had limited success in resolving slab density structure. Gravity anomaly profiles across trench/island arc complexes are characterized by a high and an adjacent low, each of large magnitude (typically ~200 mgal) and short wavelength (~200 to 300 km). As Watts and Talwani (1975) indicated, these gravity anomaly signals are so dominated by crustal effects that it is difficult or impossible to recognize the gravitational contribution of the slab. One expects the slabs to have a contribution of generally longer wavelength, by reason of their depth, than that of crustal effects. Fortunately direct observations of sea surface topography (effectively the geoid for these purposes) which are provided by Geos-3 and/or Seasat altimeters afford a more precise resolution of the gravity field's intermediate wavelength (600-4000 km) component (Chapman and Talwani, 1979). Furthermore, shorter wavelengths due primarily to near surface (e.g., crustal) effects are attenuated in the geoid

1

representation. The gravitational effects of slabs should be primarily of intermediate wavelengths and longer. Therefore the altimeter data are particularly useful in defining the density structure of slabs and in elucidating the global correlation between subduction zones and gravity highs. This correlation has been pointed out by Kaula (1972), McKenzie (1969) and Chase (1979) among others. Note that in this study sea surface topography will be assumed to represent geoid heights. This is due to the fact that oceanographic effects, constituting the difference between the geoid and the sea surface, generally should not exceed 1 or 2 meters.

A major difficulty, and in certain cases an asset, with interpreting geoid anomalies arises due to the fact that the geoid height at any one point is influenced by density variations over a relatively extensive region. Gravity anomalies on the other hand are largely due to nearby crustal density effects as indicated by the general utility of the simple Bouguer reduction. Therefore in interpreting the geoid in a given region, such as the southwest Pacific, it may be important to include slabs of the adjacent region (e.g., the New Guinea–New Britain–Solomon slabs, see below). The geoid in a given region may be particularly responsive to somewhat distant density anomalies which are not locally compensated.

On the positive side, longer wavelength density anomalies more clearly manifest themselves in the geoid. This may be seen by examining Stokes' integral formula in surface spherical harmonic form (Heiskanen and Moritz, 1967). Specifically, subducting slabs (long along strike) become substantial, perhaps dominant, contributors to geoid undulations as a direct result of their length. If one assumes that slabs worldwide possess a net linear mass anomaly (i.e., are not regionally compensated) of the order 10^{13} gm/cm, it can be seen in what follows below that slabs contribute, down to quite low degree harmonics, to the global geopotential power spectrum. In other words, slabs may

be an important source of large long wavelength gravity anomalies. As a counterexample, the South Sandwich slab is so short—along strike, that its effect on the geoid is not very noticeable.

The following are some major simplifying assumptions that have been invoked:

- The Benioff zone (zone of seismicity) completely defines the position of the anomalously dense lithospheric slab.

- Lithospheric slab thickness is not significant for these purposes and an individual slab may be considered to be condensed onto an infinitesimally thin, median surface of uniform mass per unit area.

- The contribution of crustal density variation may to a reasonable approximation be ignored.

- Thermal lithosphere associated with young marginal basins in the southwest Pacific and with the Pacific plate proper will be considered to be isostatically compensated and to have the same geoidal contribution as comparably aged normal oceanic lithosphere elsewhere (see Haxby and Turcotte, 1978, also see below).

A number of workers (including Toksoz et al., 1971, Griggs, 1972, Minear and Toksoz, 1972, Schubert et al., 1975) have developed models of the thermal behaviour of the lithosphere as it subducts into the mantle. Their results indicate that the effects of thermal contraction and elevation of mineralogical phase transitions should produce positive density anomalies in the slab. These density anomalies should vary substantially with depth. In the models that follow, density anomalies are assumed uniform with depth; discrepancies between model results and observations do not readily indicate just how density anomalies do vary with depth. Nor has it been possible to resolve any regional compensation of the slabs such as Griggs (1972) proposed.

3

In the case of the southwest Pacific, it is important to consider that different slabs have different overall density anomalies. This has been done. The model suggests that the New Hebrides slab possesses an overall average density anomaly of $+3.2 \times 10^5$ gm cm^{-2}, which is about three times the value obtained for the Tonga-Kermadec slab. Of course a unique inversion or density determination is not theoretically possible.

LINE SOURCE MODEL—GREAT CIRCLE SEGMENTS

As a prelude to the detailed models which follow, let us consider a rather idealized model of the global gravitational effect due to a slab of substantial length along strike. Consider the slab to be a line source of density, ρ_ϱ, mass per unit length. Also consider it to lie along a great circle segment of arc length $2r\psi_0$ at some depth, d, (cf., Figure 1) in a spherical Earth. The change in geoid height at any point $\vec{r}'$ is given by

$$\delta N(\vec{r}') = \frac{r G \rho_\varrho}{g} \int_{-\psi_0}^{\psi_0} \frac{d\psi}{|\vec{r}' - \vec{r}|} \tag{1}$$

where $r = |\vec{r}|$, G is the universal gravitational constant and g is gravitational acceleration at sea level. The maximum geoid height will occur over the center of the line source at $\vec{r}' = r'\hat{x}$ (i.e., $\psi', = 0$). For this case equation (1) may be rewritten as,

$$\delta N(r', \psi' = 0) = \frac{4 G \rho_\varrho r}{g(r + r')} \int_{(\pi - \psi_0)/2}^{\pi/2} \frac{d\phi}{(1 - \sin^2 \alpha \sin^2 \phi)^{1/2}}$$

where $\qquad \alpha \equiv \sin^{-1}\left(\frac{2\sqrt{rr'}}{r + r'}\right) \tag{2}$

and the substitution $\phi = (\pi - \psi)/2$ is used. The above integral is simply the difference between a complete elliptic integral of the first kind and an incomplete one. A general evaluation of potential
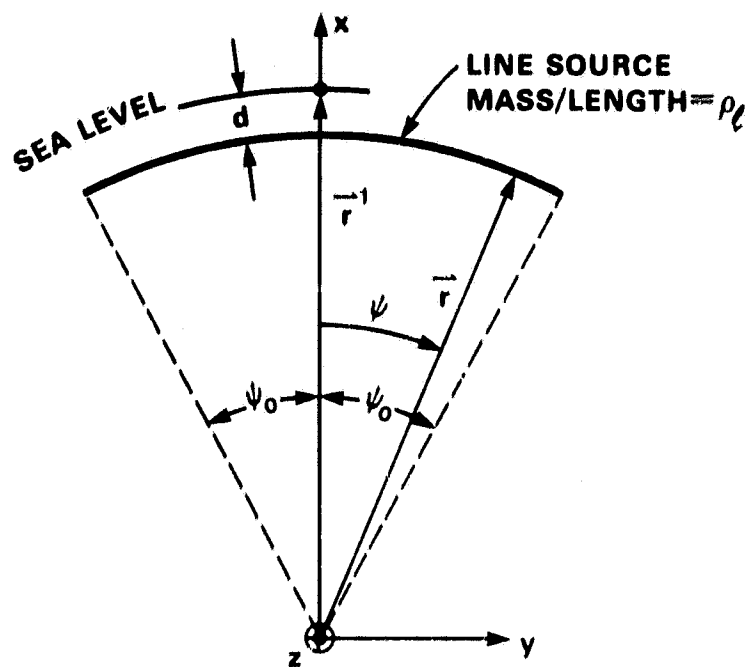
Figure 1. Geometry of a line source having the shape of a great
circle segment.

integrals of elliptic form can be found in Morrison (1980). For shallow depths ($d \ll r'$) equation (2)

may be surprisingly well approximated by the result for a straight line source (length $2r\psi_0$):

$$\delta N \, (r', 0) \; = \; \frac{2 \, G\rho_{\ell}}{g} \; \ln\left(\sqrt{1 + \zeta^2} + \zeta\right) \tag{3}$$

where
$$\zeta \equiv \frac{r \, \psi_0}{d}$$

This result is easier to evaluate. For a line source at 300 km depth, the maximum geoid height, δN,

computed using the straight line approximation (2) deviates by less than 3 percent from the actual

value of equation (1). These two results as functions of source length—are shown in normalized

form in Figure 2a.

The corresponding gravity anomalies (actually distrubances), due to this line source are given (to an excellent approximation) by the straight line result:

$$\delta g_{-x}(r', 0) \approx \frac{2\rho_\ell G}{d\sqrt{1 + (d/r\psi_0)^2}} \qquad (4)$$

where $d \ll r$. This expression is evaluated in normalized form in Figure 2b for the depth $d = 300$ km which was used in computing Figure 2a.

It is clear from Figure 2b why the two-dimensional approximation (i.e., that the structure is of infinite extent in the direction normal to the cross-section) is so useful in modelling gravity anomaly profiles which transect linear features. However, this same two-dimensional approximation (cf, Figure 2a) is not appropriate for modelling geoid undulations. The length of the structure (in the direction normal to the cross section) has a substantial influence on the magnitude of the geoid anomaly which it produces. For example, the line source model suggests that the Tonga-Kermadec slab (roughly corresponding to $\psi_0 \sim 15°$) should have a geoid anomaly amplitude about three times that of the South Sandwich slab ($\psi_0 \sim 4°$) assuming the same slab depth (actually the South Sandwich appears to be shallower) and linear mass density, ρ_ℓ. The nominal wavelength of this larger geoid anomaly will also be correspondingly larger. In contrast to the computed geoid anomalies, these two line source models should produce gravity anomaly profiles of about the same magnitude and shape. This is a simple realization of what was pointed out in the Introduction: longer wavelength mass anomalies manifest themselves more strongly than short wavelength anomalies in the geoid representation.
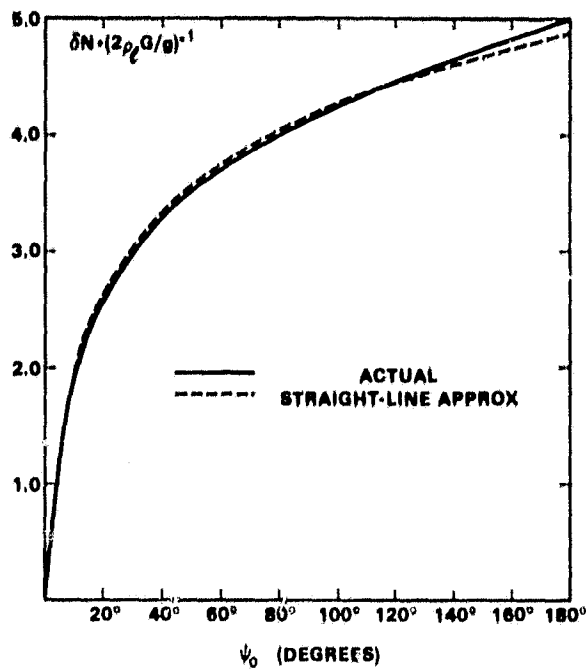
6

Figure 2a. Maximum geoid anomaly (normalized) computed as a function of angular half-length, ψ_0, of the line source. The line source is at depth 300 km in a spherical Earth.
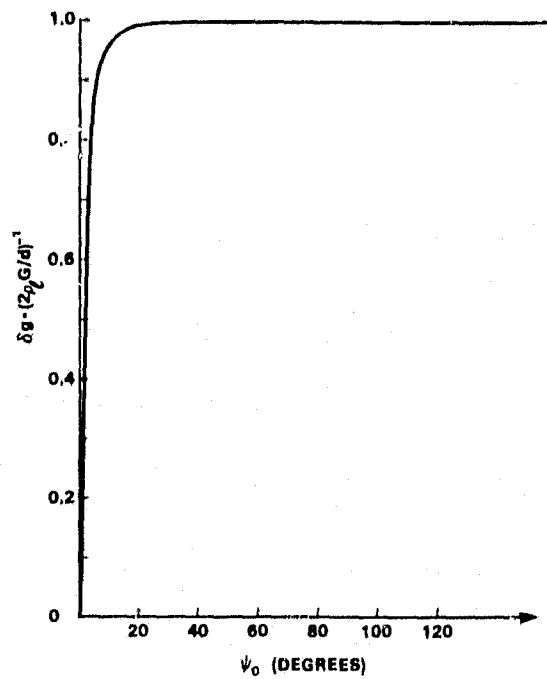

Figure 2b. The normalized gravity disturbance corresponding to Figure 2a.

Let us now consider the case of a complete great circle source (ring source); i.e., $\psi_0 = 180°$ in Figure 1. The axis or pole of this ring will be located at an arbitrary longitude, λ', and colatitude θ'. If $\theta' = 0$, for example, the ring will be equatorial. Using a derivation similar to that used by Pollack (1973) for point and cap masses, the potential due to the ring source can be represented as a spherical harmonic expansion. This potential is given at an arbitrary observation point (r, λ, θ) by:

$$\Delta V_0 (r, \lambda, \theta) = \frac{G\, 2\pi\, \rho_\ell R_0}{r} \sum_{n=0}^{\infty} \sum_{m=0}^{n} \frac{P_n(O)}{2n+1} \left(\frac{R_0}{r}\right)^n \left[\bar{R}_{nm}(\theta', \lambda') \bar{R}_{nm}(\theta, \lambda) + \bar{S}_{nm}(\theta', \lambda') S_{nm}(\theta, \lambda) \right] \quad (5a)$$

where R_0 is the radius of the ring, $\bar{R}_{nm}$ and $\bar{S}_{nm}$ are the fully normalized surface spherical harmonic functions of degree n and order m, and $P_n(O)$ are the unnormalized Legendre polynomials evaluated at $\cos \pi/2$. Excepting G, ρ_ℓ, and R_0, all symbols in (5a) conform to the definition used in Heiskanen and Moritz (1967).

Let us assign to this ring source a linear density, ρ_ℓ, which is comparable to expected density, i.e., mass per length along strike of a typical slab. Then a power spectrum can be computed and compared to an empirical measure (e.g., Kaula's rule of thumb) of the earth's geopotential power. The earth's anomalous gravitational potential, ΔV, may be expressed as:

$$\Delta V (r>R, \lambda, \theta) = \frac{-GM}{r} \sum_{n=2}^{\infty} \sum_{m=0}^{n} \left(\frac{R}{r}\right)^n \left[\bar{J}_{nm} \bar{R}_{nm}(\theta, \lambda) + \bar{K}_{nm} \bar{S}_{nm}(\theta, \lambda) \right] \quad (5b)$$

where M and R are respectively the mass and the nominal radius of the earth. Also $\bar{J}_{nm}$ and $\bar{K}_{nm}$ are the familiar coefficients of this normalized expansion. The degree variances σ_n^2 for this geopotential are given by:

$$\sigma_n^2 = \sum_{m=0}^{n} (\bar{J}_{nm}^2 + \bar{K}_{nm}^2) \quad (5c)$$

8

An empirical law due to Kaula (1968) (cf. Lambeck, 1976) provides a rough estimate of σ_n^2 for harmonics up to degree 20, according to the law:

$$\sigma_n^2 \sim (2n+1) \, 10^{-10}/n^2 \qquad (5d)$$

Figure 3 includes a plot of root variance, σ_n, given by this law. Comparable degree variances for the ring source can be determined. Excluding degree $n = 0, 1$, the expression (5a) for the potential ΔV_0 can be written exactly in the form of (5b) by defining the coefficients J_{nm}^0, K_{nm}^0 as follows:

$$\begin{pmatrix} \bar{J}_{nm}^0 \\ \bar{K}_{nm}^0 \end{pmatrix} = - \frac{2\pi \rho_\ell R_0}{M} \left(\frac{R_0}{R}\right)^n \frac{P_n(0)}{2n+1} \begin{pmatrix} \bar{R}_{nm}(\theta', \lambda') \\ \bar{S}_{nm}(\theta', \lambda') \end{pmatrix} \qquad (5e)$$

Then using (5e) ring source degree variances σ_n^2 can be computed and directly compared to the observed variances given approximately by (5d). This comparison is shown in Figure 3. The root degree variances for ring sources with two differing linear densities, ρ_ℓ, are shown. Note in computing degree variances from (5e), one can either set $\theta' = 0$ or take advantage of the orthogonality property of both $R_{nm}(\theta', \lambda')$ and $S_{nm}(\theta', \lambda')$. The ring source is placed at depth $d = 300$ km; i.e., $R_0 \cong 6070$ km where a nominal earth radius $R = 6370$ km is assumed. Also note that odd-degree variances of the ring source potential are zero.

A noteworthy aspect of Figure 3 is the near congruency of one ring source variance curve ($\rho_\ell = 2 \times 10^{13}$ gm cm^{-1}) to that of observed or empirical variance curve. Interestingly, the mass per length, which was determined below, to best fit the New Hebrides slab, works out to be approximately 2×10^{13} gm cm^{-1}. It is not clear that this density is typical of slabs worldwide, nor is it clear that this ring source model can provide a rough estimate of the power spectrum due to the global slab distribution. Overlooking these problems one might interpret this near congruency of
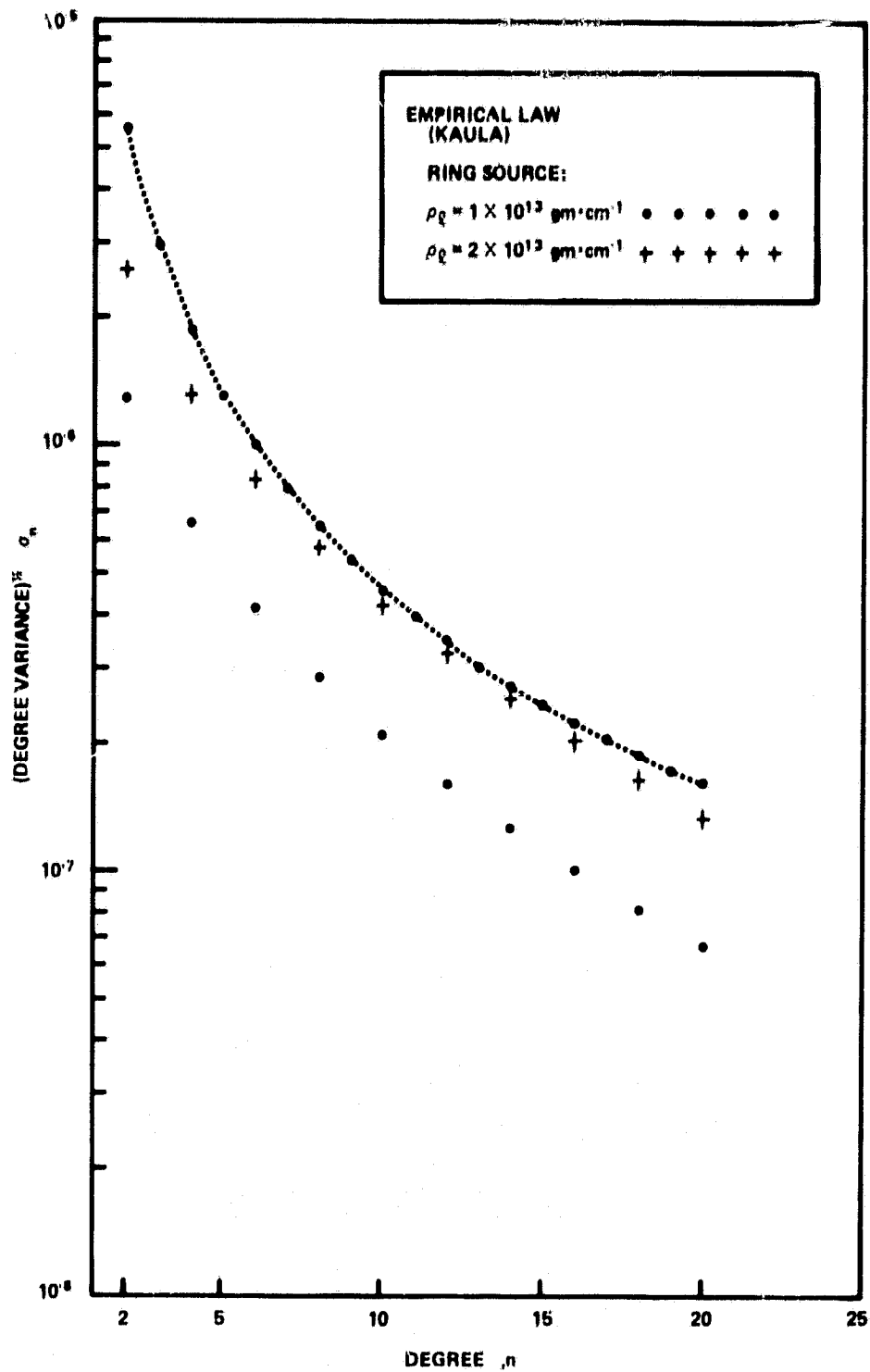
9

Figure 3. Plots of root degree variance as a function of degree for: i) Kaula's rule-of-thumb equivalent; (ii) a ring source of density $\rho_\varrho = 1 \times 10^{13}$ gm cm^{-1} and depth 300 km; (iii) a ring source of density $\rho_\varrho = 2 \times 10^{13}$ gm cm^{-1} and depth 300 km.

10

spectrum curves as an indication that slabs contribute substantial power to the observed geopotential $(4 \gtrsim$ degrees $\gtrsim 20)$.

SURFACE SOURCE MODEL

The slab is assumed to be an infinitesimally thin surface. This assumption is reasonably justified. Upward continuation of gravitational potential from slab depth to sea level washes out virtually all the manifestations of the slab's finite thickness—except perhaps those due to the slab's shallowest portions.

A surface, S, of unspecified analytical form, can be fit to the seismic data defining the Benioff zone. This slab surface will produce a geoid anomaly at $\vec{r}'$ given by:

$$\delta N(\vec{r}') = \frac{G}{g} \iint_S \frac{\sigma \, ds}{|\vec{r}' - \vec{r}'|} \tag{6}$$

where ds is an element of surface area, $\vec{r}$ is the position vector of a surface element, and σ is the mass per unit area. Let us specify that this surface, S, be polyhedral and be composed of m planar triangular facets, S_i, each having a uniform mass per unit area σ. Then equation (6) becomes:

$$\delta N(x', y', z') = \frac{G}{g} \sum_{i=1}^{m} \sigma_i \left\{ \iint_{S_i} [(x'-x)^2 + (y'-y)^2 + (z'-z)^2]^{-\frac{1}{2}} \, ds \right\} \tag{7a}$$

$$\text{or} \qquad \delta N(x', y', z') = \sum_{i=1}^{m} \delta N_i$$

$$\tag{7b}$$

By defining the apices of all facets (see Figures 4 and 5), one effectively defines the entire slab surface.
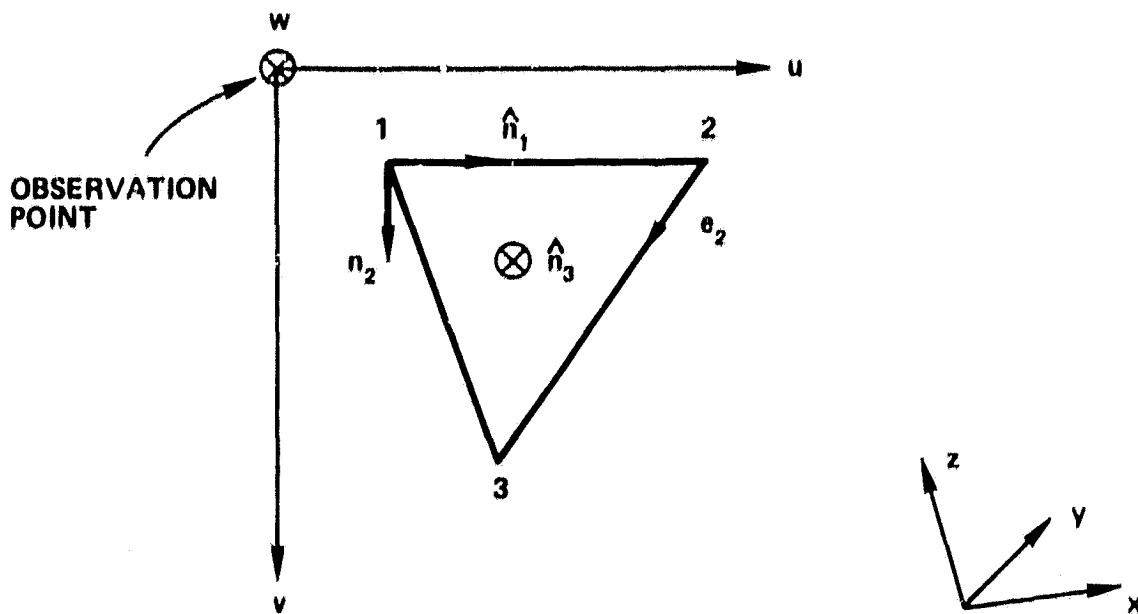
11

Figure 4. Geometry of a typical planar triangular facet showing transformed (u, v, w) and untransformed (x, y, z) coordinates systems.

The integral expression for each facet's contribution, δN_i, can be evaluated using methods applied by Chapman (1979), Barnett (1976) and Paul (1974). The integration in equation (7) can be accomplished analytically after a coordinate transformation from an arbitrary set (x, y, z) to one (u, v, w) in which the facet is coplanar with u, v (see Figure 4). This transformation is described by Paul (1974) and Chapman (1979); it consists of a rotation and a translation and is given by:

$$\begin{pmatrix} u \\ v \\ w \end{pmatrix} = \begin{pmatrix} n_{11} & n_{12} & n_{13} \\ n_{21} & n_{22} & n_{23} \\ n_{31} & n_{32} & n_{33} \end{pmatrix} \begin{pmatrix} x - x_0 \\ y - y_0 \\ z - z_0 \end{pmatrix} \tag{8}$$

where (x_0, y_0, z_0) is the position of the observation point and n_{ij} is the familiar direction cosine matrix. For example, n_{12} is y component of the unit vector $\hat{n}_1$. Note from Figure 4 that $\hat{n}_3 = \hat{n}_1 \times \hat{e}_2$ and $\hat{n}_2 = \hat{n}_3 \times \hat{n}_1$. Term δN_i of (7b) becomes—in transformed coordinates—

$$\delta N_i = \frac{G}{g} \sigma_i \int_{\Delta S_i} \frac{du\, dv}{[u^2 + v^2 + w^2]^{\frac{1}{2}}} \tag{9}$$
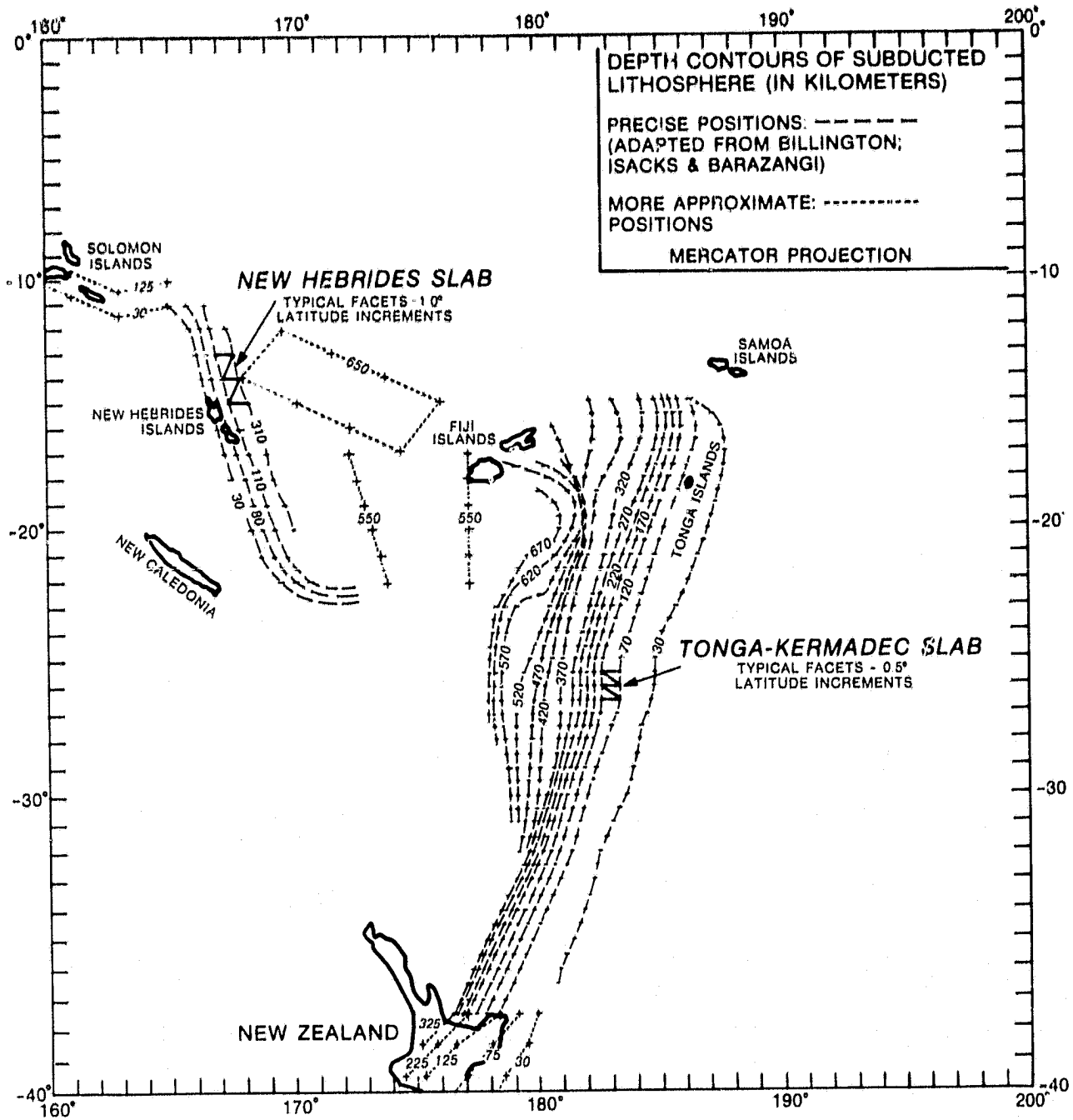
12

Figure 5. Contours defining the position of the slabs. Slabs are considered to be infinitesimally thin. Crosses define apices of individual blocks, each of which comprises two triangular facets. Finely dashed line defines slabs (segments) which correspond to precisely located Benioff zones. See text for details.

13

By applying Stokes' theorem to the integral in equation (9), it can be rewritten as:

$$\delta N_i = \frac{G\sigma_i}{g} \int_c \ell n \left[u + \sqrt{u^2 + v^2 + w^2} \right] dv \qquad (10)$$

where C is the perimeter closed contour and integration is performed in a right-handed positive $\hat{w}$ sense. For the triangular facet shown in Figure 4, one can integrate (10) and obtain:

$$
\delta N_i = \frac{G\sigma_i}{g} \left\{ v_1 \, \ell n \left[\frac{u_1 + R_1}{u_2 + R_2} \right] + \frac{\beta_2}{(\alpha_2^2 + 1)^{\frac{1}{2}}} \ell n \left[\frac{\alpha_2 \beta_2 (\alpha_2^2 + 1)^{-\frac{1}{2}} + (\alpha_2^2 + 1)^{\frac{1}{2}} V_3 + R_3}{\alpha_2 \beta_2 (\alpha_2^2 + 1)^{-\frac{1}{2}} + (\alpha_2^2 + 1)^{\frac{1}{2}} V_1 + R_2} \right] \right.
$$
$$
+ \frac{\beta_3}{(\alpha_3^2 + 1)^{\frac{1}{2}}} \ell n \left[\frac{\alpha_3 \beta_3 (\alpha_3^2 + 1)^{-\frac{1}{2}} + (\alpha_3^2 + 1)^{\frac{1}{2}} v_1 + R_1}{\alpha_3 \beta_3 (\alpha_3^2 + 1)^{-\frac{1}{2}} + (\alpha_3^2 + 1)^{\frac{1}{2}} v_3 + R_3} \right]
$$
$$
+ w \left[\tan^{-1} \left(\frac{\alpha_2 w^2 - \beta_2 v_3}{w R_3} \right) - \tan^{-1} \left(\frac{\alpha_2 w^2 - \beta_2 v_1}{w R_2} \right) \right.
$$
$$
\left. \left. + \tan^{-1} \left(\frac{\alpha_3 w^2 - \beta_3 v_1}{w R_1} \right) - \tan^{-1} \left(\frac{\alpha_3 w^2 - \beta_3 v_3}{w R_3} \right) \right] \right\} \qquad (11)
$$

where (u_1, v_1, w), (u_2, v_1, w), and (u_3, v_3, w) are the locations of apex 1, 2, and 3, respectively (note $v_2 = v_1$ and $w_3 = w_2 = w_1 \equiv w$) and where:

$$\alpha_2 = (u_3 - u_2/(v_3 - v_1) ,$$
$$\alpha_3 = (u_1 - u_3)/(v_1 - v_3) ,$$
$$\beta_i = u_i + \alpha_i v_i , \quad i = 2, 3,$$
$$R_i = (u_i^2 + v_i^2 + w^2)^{\frac{1}{2}} , \quad i = 1, 2, 3.$$

This result (11) is similar to that obtained by Chapman (1979) and Barnett (1976) for a three-dimensional body; the only difference being that this result is developed for a polyhedral surface source.

14

Surfaces representing the Tonga-Kermadec slab and the New Hebrides slab are shown in Figure 5. The Tonga-Kermadec slab is blocked in 0.5° latitude intervals along each pair of adjacent depth contours. The contours are adapted from those of Billington (1979). Each block is composed of two triangular facets. The facets on a pair of typical blocks are shown in Figure 5. All other blocks are similarly facetted; this is not shown. There are a total of 944 triangular facets in this slab. The shallow portion ($\leqslant$ 310 km depth) of the New Hebrides slab is blocked in 1.0° latitude intervals and totals 68 triangular facets. These depth contours are adapted from those of Isacks and Barazangi (1977).

The depth contours of Billington (1979) and Isacks and Barazangi (1977) define the position of the top of the Benioff zone. In our slab model (see Figure 5), these seismicity contours have been shifted using a slab half-thickness of 25 km and a single overall average slab dip which is applied to all contour excepting the trench axis contour. The trench axis contour is shifted directly downward.

It is important to include continuations of the Benioff zone westward from the northern New Hebrides and southward from the southern Kermadec. These zones (slabs) are relatively distant from the points at which their geoid contribution is to be computed. Over such distances, short wavelength gravitational effects are washed out and only crude models (coarse blocking) are needed. The Benioff zone(s) of the Solomon-New Britain-New Guinea region has been crudely represented using either one or two blocks (i.e., one or two depth intervals) for each 2° longitude interval from 165°E westward to 135°E (see Figure 5). These two-dimensional blocks represent approximate fits to the seismic zone determinations of Pascal (1979) and Johnson and Molnar

15

(1972). Similarly, a crude fit to the seismicity distributions derived by Hamilton and Gale (1968) for North Island, New Zealand, provide an extension of the southern Kermadec slab to 41.5°S latitude. A portion of this fit is shown in Figure 5 (high-frequency-dash contours).

A rectangular contour at 650 km depth under the northern Fiji plateau encloses three blocks which crudely fit the seismic zone detailed by the Isacks and Barazangi (1977) and Pascal et al (1978). Both of these papers suggest that this zone may coincide with a remnant segment of sub-ducted Pacific plate. The Vitiaz trench is thought to be a legacy of this extinct subduction zone. This rectangular segment will be lumped with the Tonga-Kermadec slab when assigning density anomalies and computing geoids.

The 550 km contours under the southern Fiji Plateau define a trapezoidal slab segment which roughly fits a seismic zone detailed by Barazangi and Isacks. Both they and Pascal et al (1978) suggest that this zone probably is related to ongoing New Hebrides subduction. Therefore this 550 km deep segment will be lumped with the shallower New Hebrides slab in assigning densities and computing geoids. Evidence that there is indeed a discontinuity (as idealized in Figure 5) between the shallow and deep slab portions is presented by Barazangi et al (1973).

Theoretical geoid anomalies computed from this slab model are shown in Figures 9-11. Comparisons with observations are contained in the Results section. It can be seen that the character in the computed geoid anomalies is largely attributable to the Tonga-Kermadec and shallow New Hebrides slabs. In other words, the more precisely located slabs (Benioff zones), not the crudely located slabs, provide the computed geoid with its important shape and character.

16

A MODEL OF THERMAL LITHOSPHERE ASSOCIATED WITH MARGINAL BASINS

Recent studies (Haxby and Turcotte, 1978; Haxby, 1980; Crough, 1979) have shown that observed geoid heights tend to vary systematically with the age of normal oceanic lithosphere. In particular, Haxby and Turcotte (1978) showed that observed geoid heights tend to decrease linearly with increasing lithospheric age out to 80 m.y.B.P. in good agreement with the half-space simple conductive cooling model. Crough (1979) showed that there are significant geoid height changes across fracture zones which separate lithospheric segments of differing ages. A similar age contrast exists across deep ocean trenches. It appears that for a number of trenches, geoid heights increase as the observer crosses from areas seaward of the trench to those landward of the trench. Part of this height increase is due to the contrast between the young, thin lithosphere of the marginal basins and the typically older, thicker oceanic lithosphere seaward of the trench.

It will be assumed a priori, that thermal lithosphere associated with four marginal basins (see Figure 6) of the southwest Pacific can be modelled as normal oceanic lithosphere. More exactly, the following relations apply: the depth-age relation from thermal isostasy:

$$w = w_R + \frac{2\rho_m \alpha (T_m - T_o)}{(\rho_m - \rho_w)} \left(\frac{\kappa t}{\pi}\right)^{1/2} \tag{12}$$

due to Davis and Lister (1974), among others, and the associated geoid height-age relation

$$\Delta N = - \frac{2\pi G}{g} \rho_m \alpha (T_m - T_o) \kappa \left[1 + \frac{2\rho_m \alpha (T_m - T_o)}{(\rho_m - \rho_w) \pi} \right] (t - t_r) \tag{13}$$

due to Haxby and Turcotte (1978). In the two preceding equations, T_m is the initial isothermal mantle temperature; T_o is the invariant surface temperature; ρ_m is mantle density at temperature T_m; ρ_w is seawater density; κ is the mantle thermal diffusivity; α is the volumetric coefficient of
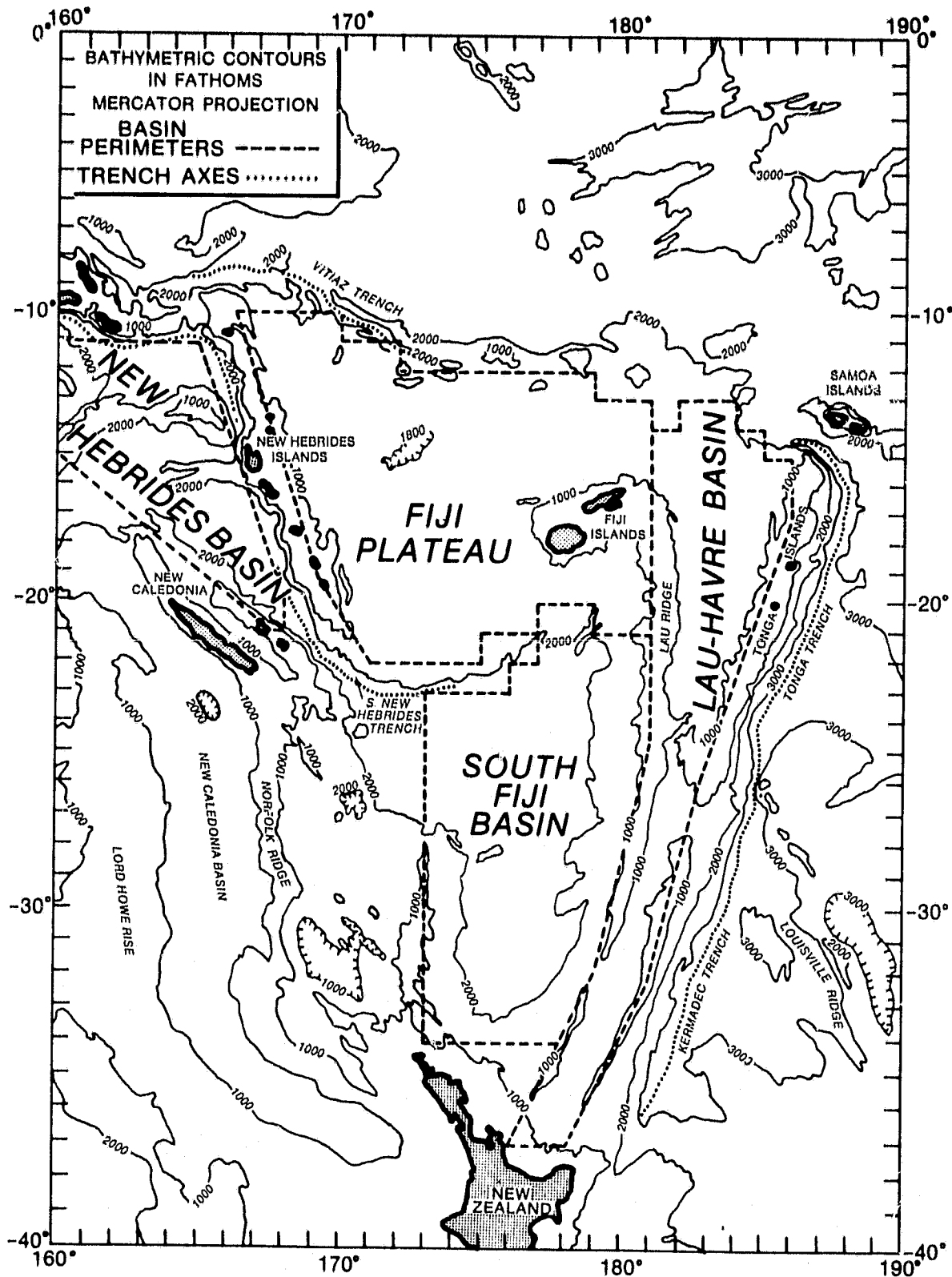
17

Figure 6. Dashed perimeters define the extent of four marginal basins. These basin definitions are used in constructing the two-layer doublet shell model of the thermal lithosphere. See text and Table 1 for details.

18

thermal expansion; w_R is the depth to the right crest; t is the particular lithospheric age; and t_R is age of lithosphere used as a reference (i.e., corresponds to zero geoid height).

Marginal basins differ distinctly in character from normal oceanic lithosphere; although they both evolve via crustal extension. Certainly the assumption of similarity, outlined above, is somewhat tenuous. For an individual marginal basin, it is quite difficult to observe the depth-root age relation (12). This difficulty is perhaps due to characteristically rough topography (cf., Karig et al., 1978). However, the South Fiji Basin, the Lau-Havre Basin, and the Fiji Plateau (see Figure 6) each have paired values of average depth—average age which fall nearly on the depth-age curve for the North Atlantic or North Pacific (see depth anomalies in Table 1). Other marginal basins, such as the Mariana Trough, lying outside this study's region of interest, are substantially deeper, on average, than comparably-aged normal oceanic lithosphere (Karig et al., 1978). The rough agreement between the normal oceanic lithosphere's age depth relation and that of the marginal basins in this study provides justification for applying the model given in (13).

In computing a map of geoid anomalies due to marginal basin/oceanic lithosphere contrast, all geoid heights refer to a zero datum which corresponds to the Pacific plate seaward of the Tonga-Kermadec trench. In other words, the Pacific plate reference age, t_r, in (13) is 75 m.y.B.P. Equation (13) will not be used explicitly to compute geoid anomalies. This expression is an approximation which is valid for long wavelength features (> 200 km).

As Haxby and Turcotte (1978) have indicated, it can be expressed as

$$\Delta N = \frac{2\pi G}{g} \mu \tag{14}$$

19

Table 1.

Table 1.
Marginal Basins of the Southwest Pacific

Basin	*Period of Activity (10^6 yrs)	**Mean Depth-$\overline{W}$ (km)	Representative Age-t (10^6 yrs)	Dipole Moment, μ (gm cm^{-1})	Depth Anomaly (km)
Fiji Plateau	0-3[1]/0-9 BP[2]	2.9^6	2.0/6.0	2.73×10^{12}	0.0/+0.3
South Fiji	28-35 BP[3]	4.6^7	31.5	1.63×10^{12}	-0.1
Lau Havre	0-3.5 BP[4]	2.6^8	2.3	2.71×10^{12}	+0.3
New Hebrides	45-52 BP[5]	<4.9	48.5	0.99×10^{12}	—

*Periods of activity from: 1. Cherkis et al (1978); 2. Falvey (1975); 3. Watts and Weissel (1977); 4. Weissel (1977); 5. Weissel et al (1977).
**Mean depths from: 6. and 7. Karig (1971); 8. Toksoz and Bird (1977).

where μ is the first moment, in depth, of the density distribution. Comparison with (13) yields the expression for moment

$$\mu = \rho_m \alpha (T_m - T_o) \kappa \left[1 + \frac{2\rho_m \alpha (T_m - T_o)}{(\rho_m - \rho_w) \pi} \right] (t_r - t) \qquad (15)$$

The geoid anomaly map (e.g., Figure 7) is computed by constructing an equivalent doublet shell of moment, μ, as given above. The moment for each of the four basins is listed in Table 1. The dipole moment can be decomposed into a source term, σ, given by

$$\sigma = 2\rho_m \alpha (T_m - T_o) \left(\frac{\kappa}{\pi} \right)^{1/2} (t_r^{1/2} - t^{1/2}) \qquad (16a)$$

and a separation distance d given by

$$d = \frac{(\pi \kappa)^{1/2}}{2} \left[1 + \frac{2\rho_m \alpha (T_m - T_o)}{(\rho_m - \rho_w) \pi} \right] \frac{(t_r - t)}{(t_r^{1/2} - t^{1/2})} \qquad (16b)$$
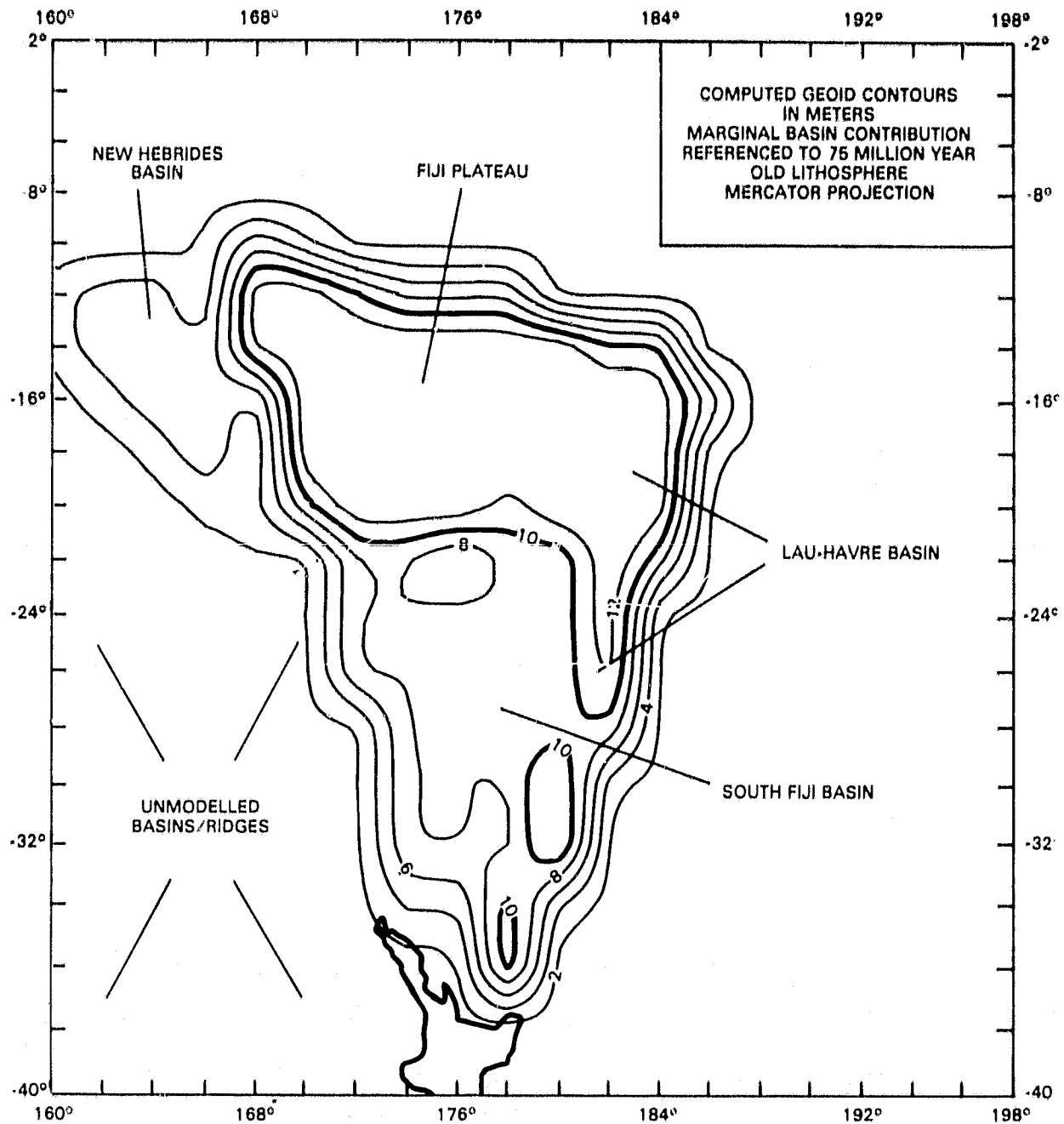
Figure 7. Contour map of geoid anomalies in meters computed from the doublet shell model of the young thermal lithosphere of the four marginal basins. Referenced to the 75 m.y. old lithosphere of the Pacific plate. See text and Table 1.

such that $\mu = \sigma d$. Two polyhedral surfaces are used to form the doublet shell. For each of the four basins in Table 1, the upper surface of areal density $+\sigma$ (see equation 16a) is placed at mean depth $\overline{w}$. The lower surface of density $-\sigma$ is placed at depth $\overline{w} + d$, where d is given by 16b. The geoid anomaly map (Figure 7) is then computed using the facet integration ($1° \times 1°$ blocking) and summation described in the preceding section.

This technique results in a smooth geoid even at the edges of the basins. If equation (13) were applied directly, the resultant geoid would have discontinuities at the edge of the basin. The geoid computed from the doublet shell does not contain the spurious high frequency components which will occur in a geoid computed directly from (13).

In calculating the dipole moment, μ, separation distance, d, theoretical depth, w, etc. for each basin a representative age (t in Table 1) is used. Also Parsons and Sclater's (1977) best fitting parameters (North Pacific determinations) were used. They are: $\rho_m = 3.33$ gm cm^{-3}, $\kappa = 8.0 \times 10^{-3}$ cm^2.s^{-1}, $T_m - T_0 = 1333°$ and $\alpha = 3.3 \times 10^{-5}$ °C^{-1}. The representative age is derived from published studies of the particular basin's magnetically expressed history (see Table 1). It is not a mean age. It is the age associated by the age-depth relation (12) with the predicted mean depth. The predicted mean depth is computed using (12) and assuming a uniform spreading rate. Note that actual mean depths are shown in Table 1. These depths are due to Karig (1971) and Toksoz and Bird (1977). A mean depth for the New Hebrides basin was not included, as this basin's apparent complexity made a meaningful determination difficult.

Note that map coverage in Figure 7 is not complete. There are a number of different basins in this $40° \times 40°$ region which have not been sufficiently studied to obtain estimates of the thermal

22

lithosphere's age. Therefore, these regions (e.g. the southwestern corner) appear as gaps—i.e., they are shown as areas of zero geoid anomaly or lithospheric age contrast.

Note also that the effect of a young basin on geoid heights is clearly localized. This results from the assumption of an isostatically compensated thermal lithosphere.

RESULTS

Figure 8 contains a map of sea surface topography in the southwest Pacific derived from Seasat-I altimeter data. This map was constructed from data obtained between July 28 and August 15, 1978 and is due to J. G. Marsh et al (1980). Heights are referenced to an ellipsoid of flattening, $F = 1/298.255$, and semi-major axis, $a = 6,378,140$ meters. Small crossover height differences permitted direct contouring of the along-track data into map form. Tides were not explicitly removed in obtaining the heights in this map. The contribution of oceanographic effects to this representation of sea surface topography can be expected to be generally less than one meter in magnitude. For the purposes of this study, the map (Figure 8) may be considered to represent the marine geoid. Wavelengths shorter than 200 km are effectively filtered out of this map.

Figure 9 represents the computed geoid anomaly due to the surface source model (as previously described) of the regional slab distribution. The assumed density anomalies are: (i) for the Tonga-Kermadec slab, 1.0×10^5 gm cm⁻² and (ii) for the New Hebrides slab, 3.2×10^5 gm cm⁻². In this case, the New Guinea-New Britain-Solomon (NG-NB-S) slabs of the adjacent region are assigned the same density as the Tonga-Kermadec. As explained earlier, deep slab segments under the northern and southern Fiji Plateau are lumped, for density assignment purposes, with the Tonga and New Hebrides slabs respectively.
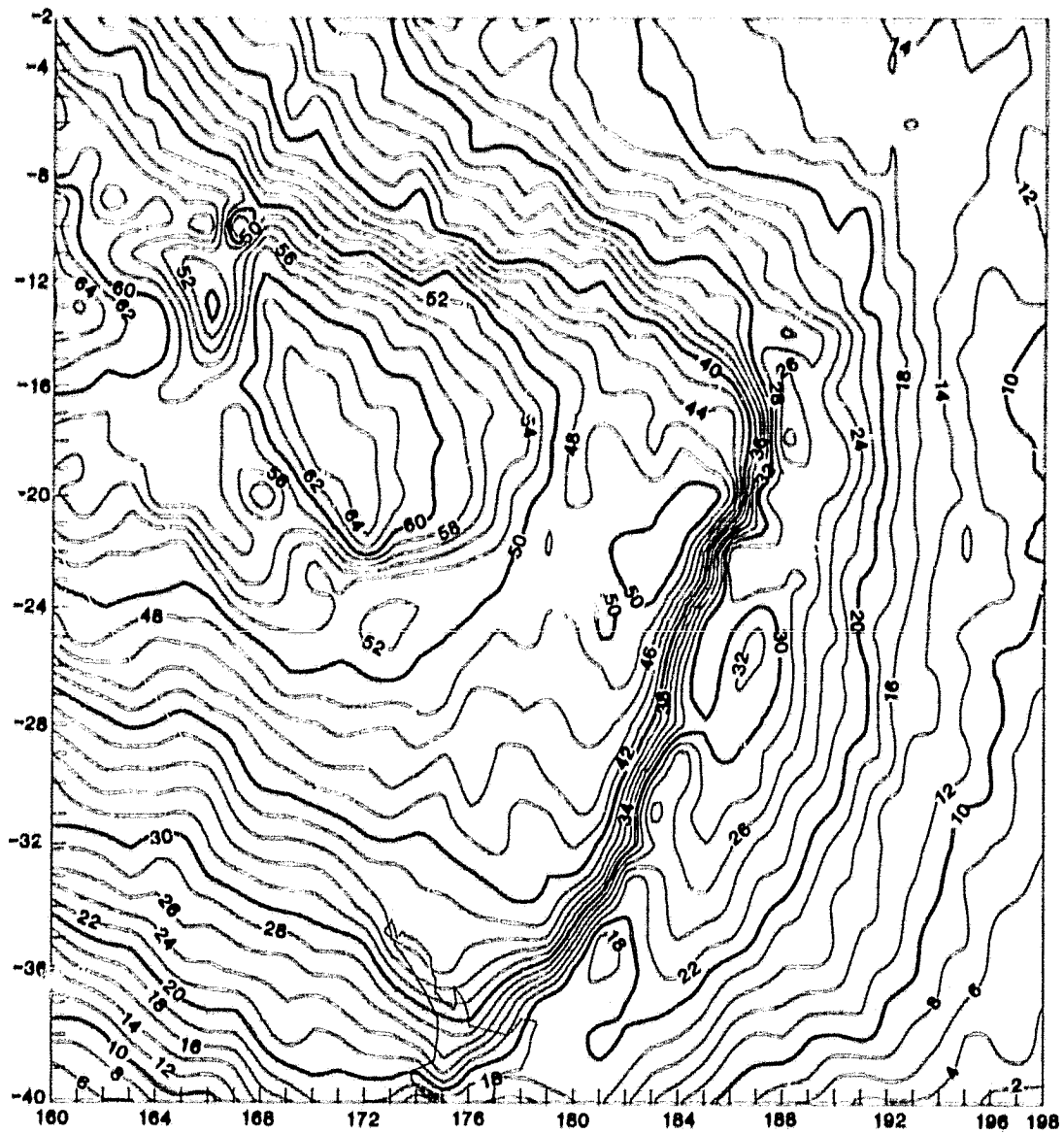
Figure 8. Contour map of sea surface heights in meters computed from Seasat altimeter data (due to Marsh, 1980). Data acquired: July 28, 1978 to August 15, 1978. Reference ellipsoid: $f = 1/298.255$; $a = 6,378,140$ m.
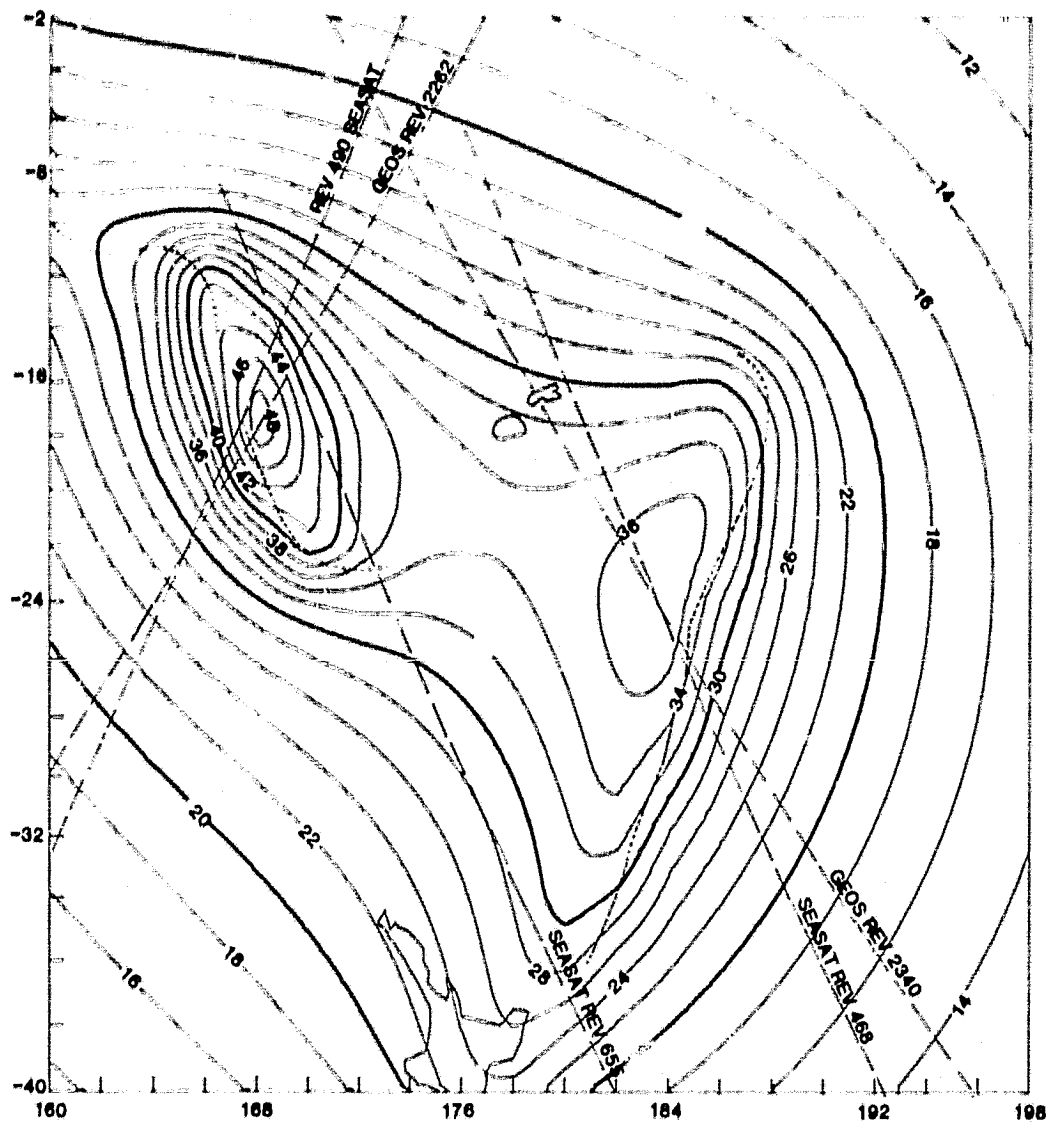
Figure 9. Computed geoid height contours in meters due to the slab model. Densities are: 1.0×10^5 gm cm^{-2} for the Tonga-Kermadec and NG-NB-S slabs; 3.2×10^5 gm cm^{-2} for the New Hebrides slab. Dashed lines are ground tracks of satellite passes used in Figure 12. Dotted lines show the positions of the Tonga-Kermadec and New Hebrides trench axes.

In comparing these regional computed geoid anomalies (Figure 9) with the observed sea surface (Figure 8), agreement in shape and character can be easily seen. Note in particular that the twin local maxima at longitude ~169°E, latitude ~18° and longitude ~184°E, latitude ~22°. As will be seen in Figures 12a-12e, one obtains a much better agreement by including the geoidal effect of lithospheric age contrast between young marginal basin areas and those of older Pacific lithosphere. Furthermore, this model ignores crustal and bathymetric effects. To some degree, such effects are represented in the sea surface map. For example, weak lows tend to be positioned over the Tonga-Kermadec and New Hebrides trench axis.

The significant character in the computed geoid (Figure 9) is largely attributable to those slabs (slab segments) which possess more precise fits. These fits result from Benioff zone determinations of Billington (1979) and Isacks and Barazangi (1977); they are described in Figure 5. The geoidal effect of these slabs is shown in Figure 10. Clearly the twin maxima in the preceding computed geoid (Figure 9) arise due to these slabs.

Figure 11 shows another computed regional geoid. This computation differs from that of Figure 9 only in that the density of the New Guinea-New Britain-Solomon (NG-NB-S) slab complex has been raised from 1.0 to 2.6 X 10^5 gm cm^{-2} and the density of the New Hebrides slab lowered from 3.2 to 2.6 X 10^5 gm cm^{-2}. This geoid is comparable to that of Figure 9 except that there is less closure of the contour lines in the northwest corner of this map (Figure 11). In this particular aspect the geoid of Figure 11 provides slightly better agreement with the observed geoid. In fact, global sea surface maps or geoids display a rather pronounced high over the New Guinea area. This suggests that the choice of a higher (2.6 X 10^5 gm cm^{-2}) nominal density anomaly for the NG-NB-S slabs may be closer to correct. However, the geoids computed in Figures 9 and 11 are not
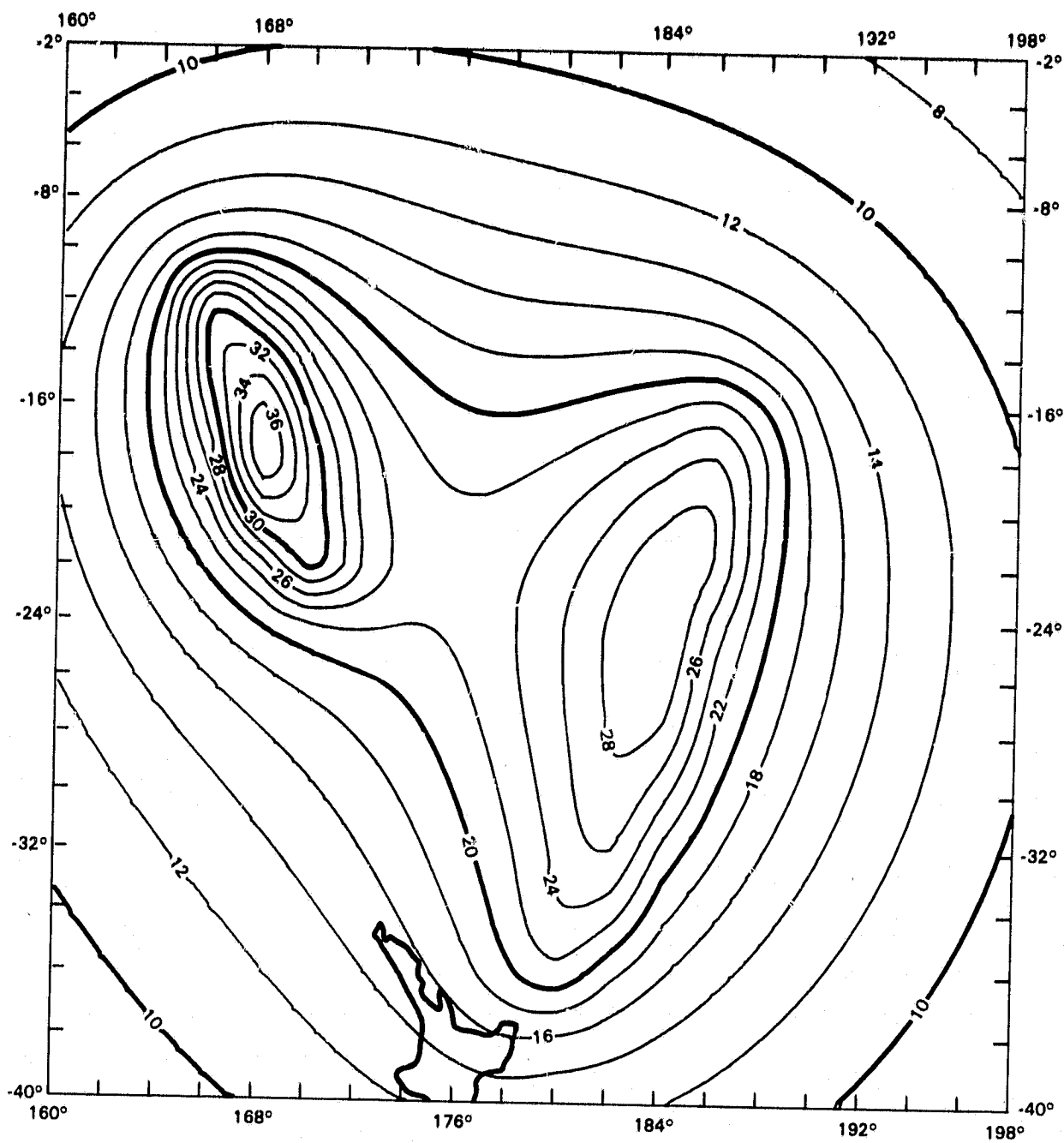
Figure 10. Computed geoid height contours (in meters) due to the precisely located slab sgements. Densities as in Figure 9.
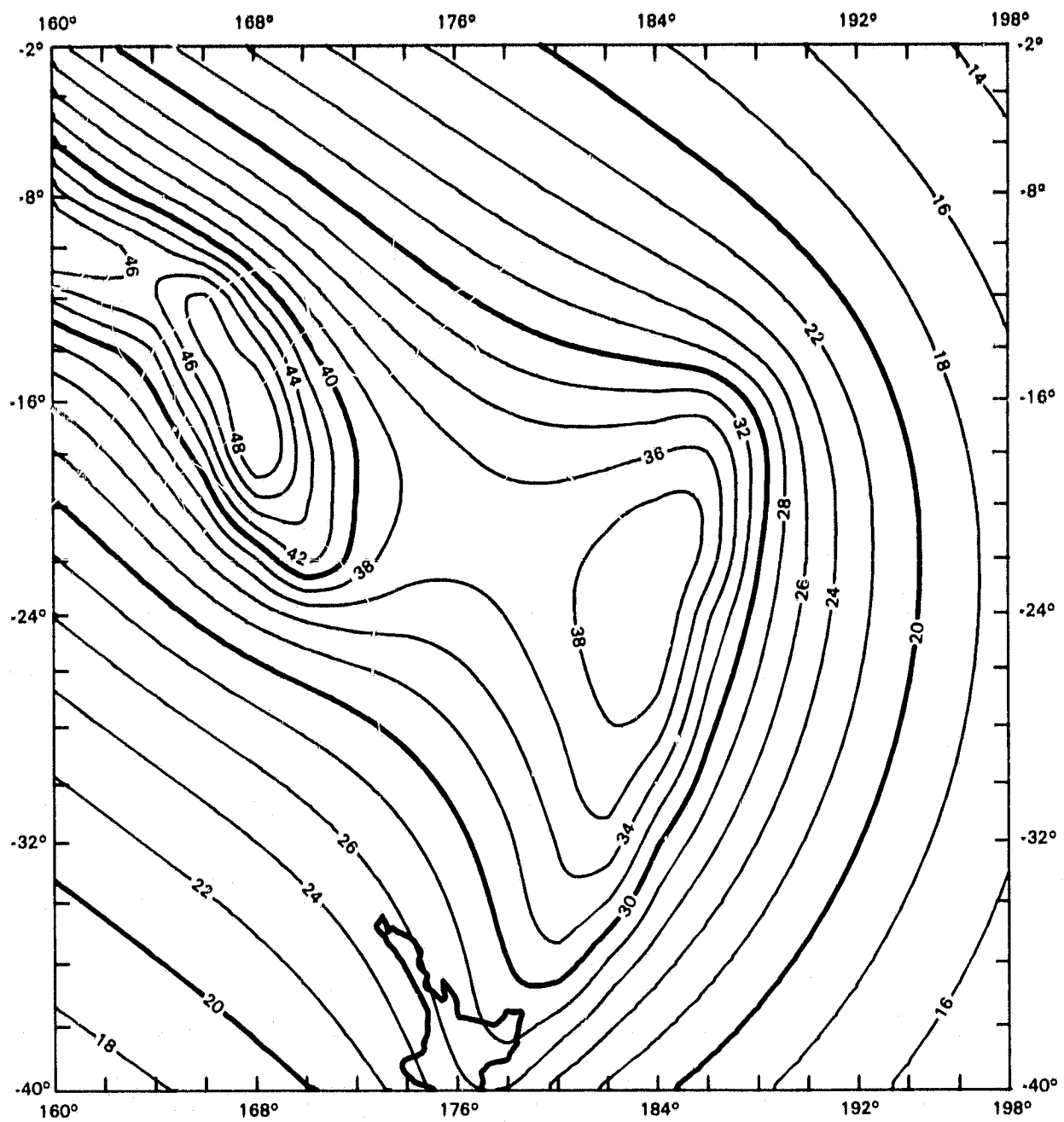
Figure 11. Computed geoid heights in meters due to the slab model. Densities are: 1.0×10^5 gm cm^{-2} for the Tonga-Kermadec slab; 2.6×10^5 gm cm^{-2} for the New Hebrides and NG-NB-S slabs.

sensitive to the particular density anomaly selected for these slabs. To obtain a reasonable density anomaly estimate for the NG-NB-S slabs, one must also study the sea surface topography in their immediate vicinity.

As indicated above, the effect of age contrast between the lithosphere underlying young marginal basins and that underlying deeper ocean floor should also be included in a model of the regional geoid. Ideally, the geoidal undulations due to this effect should be superposed on the computed effect of slabs. However, sufficient data is not available to compute this age contrast effect for the entire $40° \times 40°$ region under study. In the preceding section, four marginal basins are modelled (see Figure 7). A number of basins in this region are unmodelled; Figure 7 contains information gaps. It is therefore more useful to compute the geoidal contribution of these two effects (age contrast and anomalously dense slabs) in profiles along selected subsatellite tracks and then superpose them. This has been done. Comparisons with along-track sea surface profiles are shown in Figures 12a-12e.

The ground track map of these five satellite passes is included in Figure 9. Figures 12a-12c are Seasat I passes; Figures 12d and 12e are Geos-3 passes. The model geoids are quite smooth; they were computed at every third or fourth observation point. Observed data points are spaced, after smoothing, at 1 second intervals. Sea heights for the two Geos-3 passes are referred to an ellipsoid of semimajor axis 6378140 m and flattening 1/298.255. The Seasat passes are referred to an ellipsoid of semimajor axis 6378140 m and flattening 1/298.257 An ocean tide model correction has been applied to Seasat heights but not to Geos-3 heights. In computing model geoids in Figures 12a-12e, the same slab density anomalies (1.0 and 3.2×10^5 gm cm^{-2}) used in Figure 9 were employed.
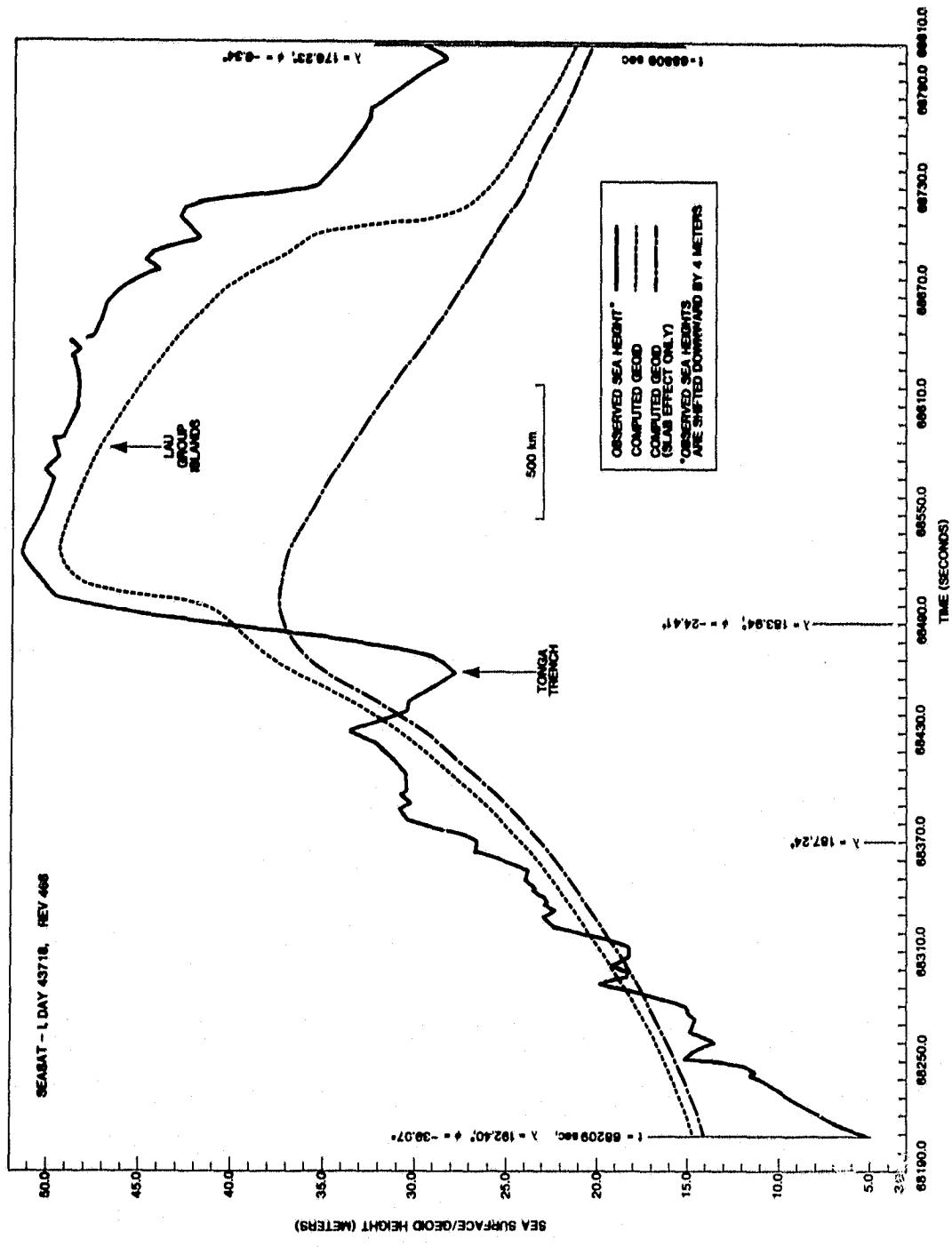
Figure 12a. Comparison of model results with altimetric height profiles. Dashed line represents a superposition of geoid heights from the slab model of Figure 9 and heights from the thermal lithosphere model of Figure 7. The long dashed-short dashed line represents just the slab model result. Groundtracks are shown in Figure 9. Sea height profile is from the Seasat altimeter.
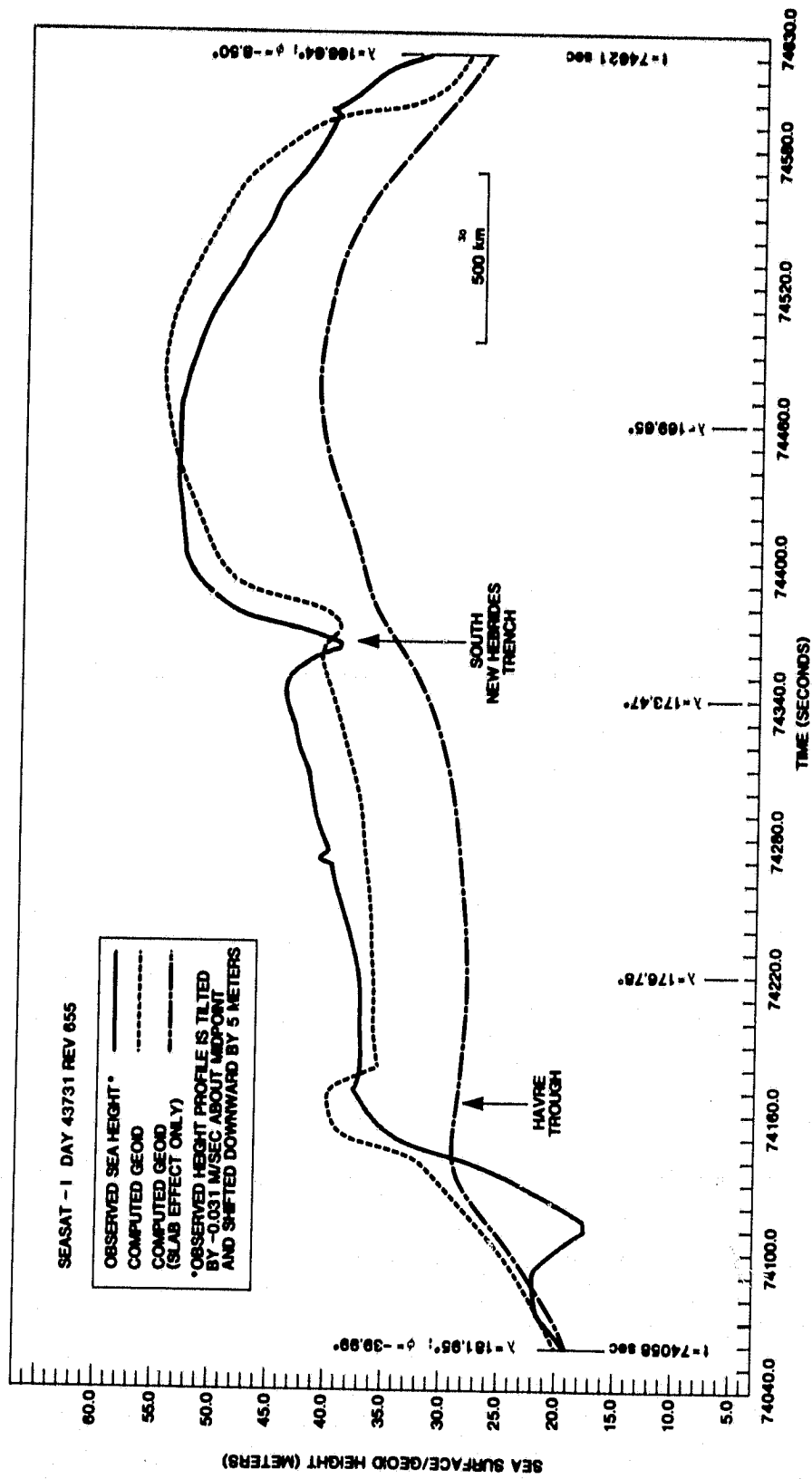
Figure 12b. See Figure caption 12a. Sea height profile is from the Seasat altimeter.
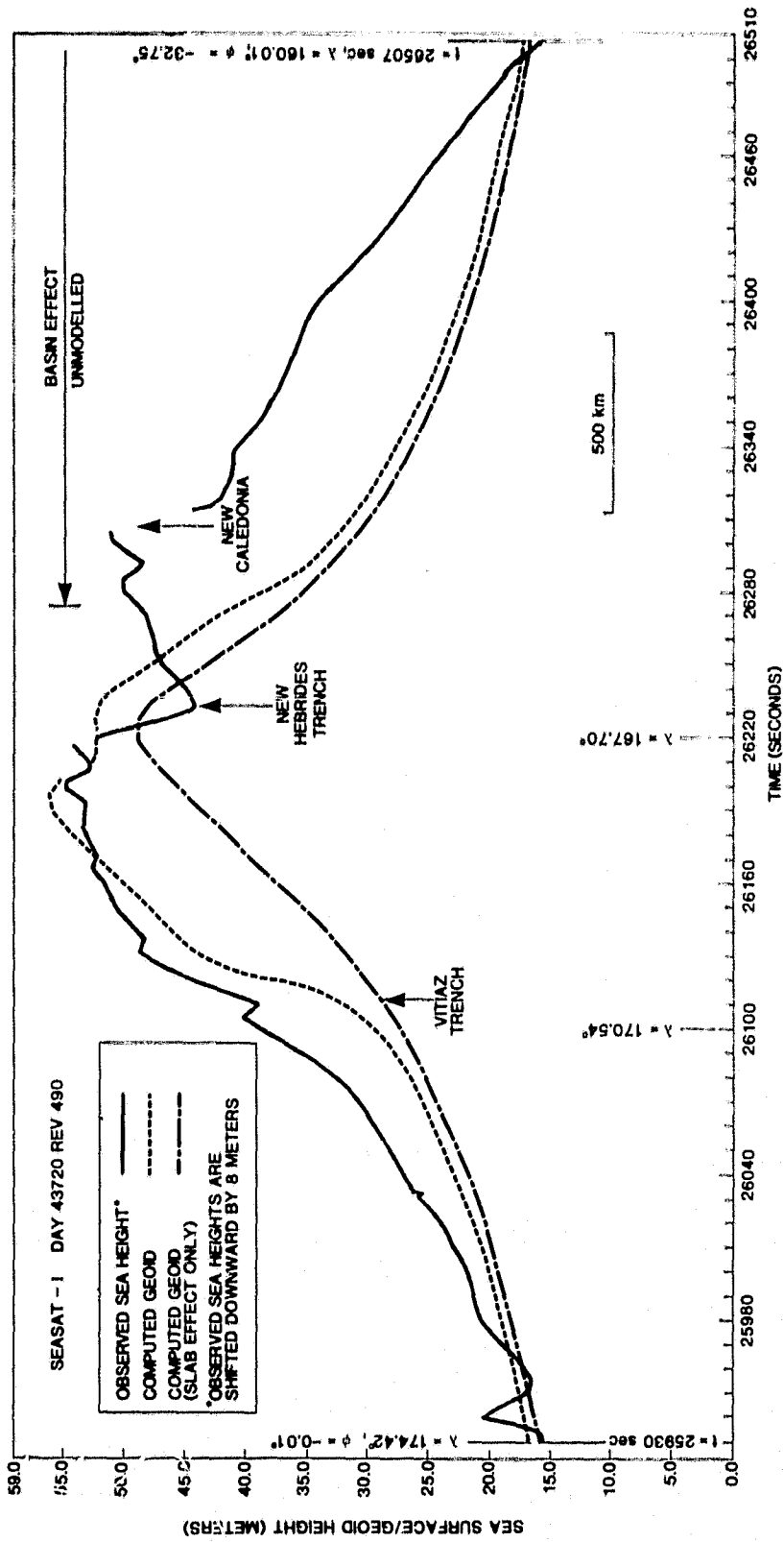
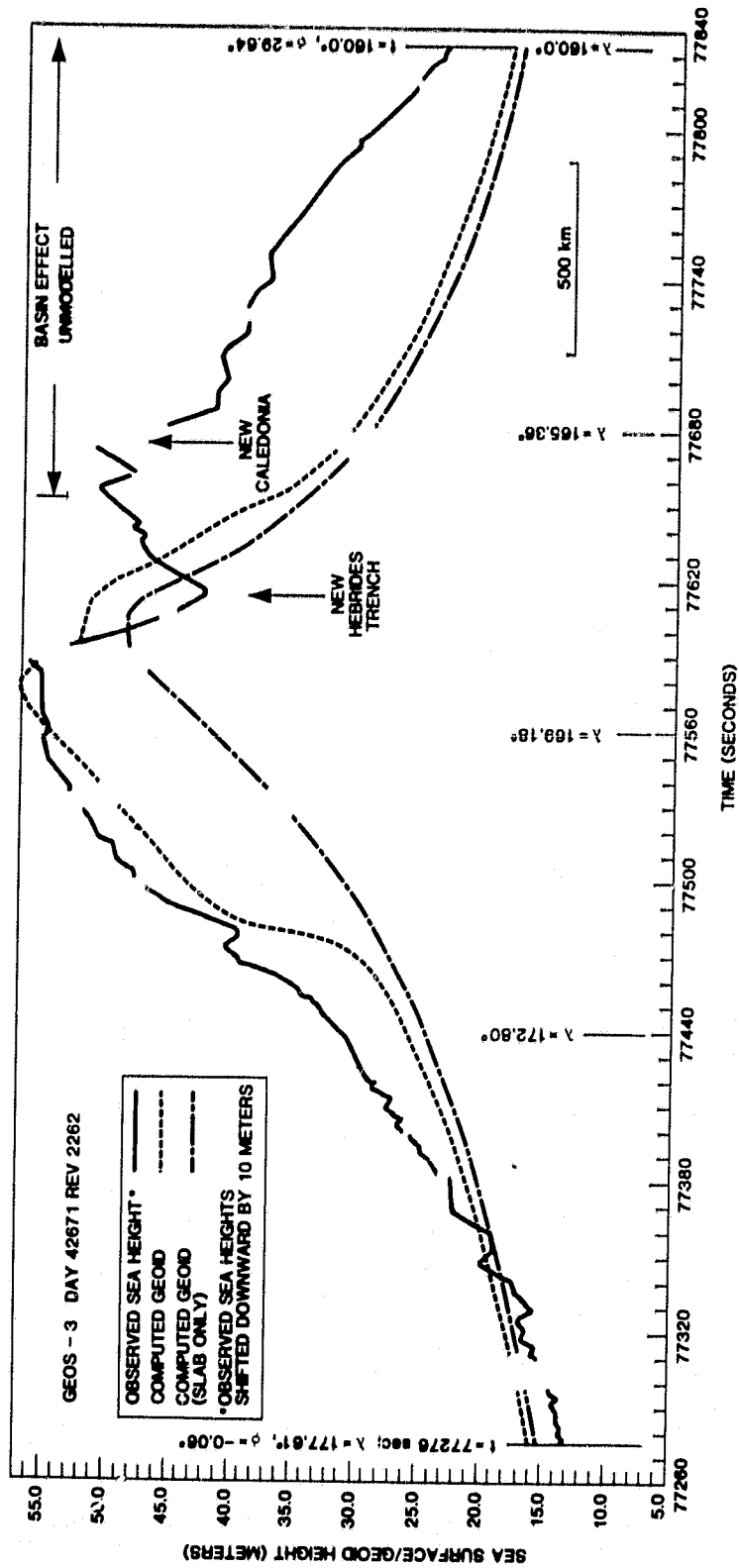Figure 12c. See Figure caption 12a. Sea height profile is from the Seasat altimeter.

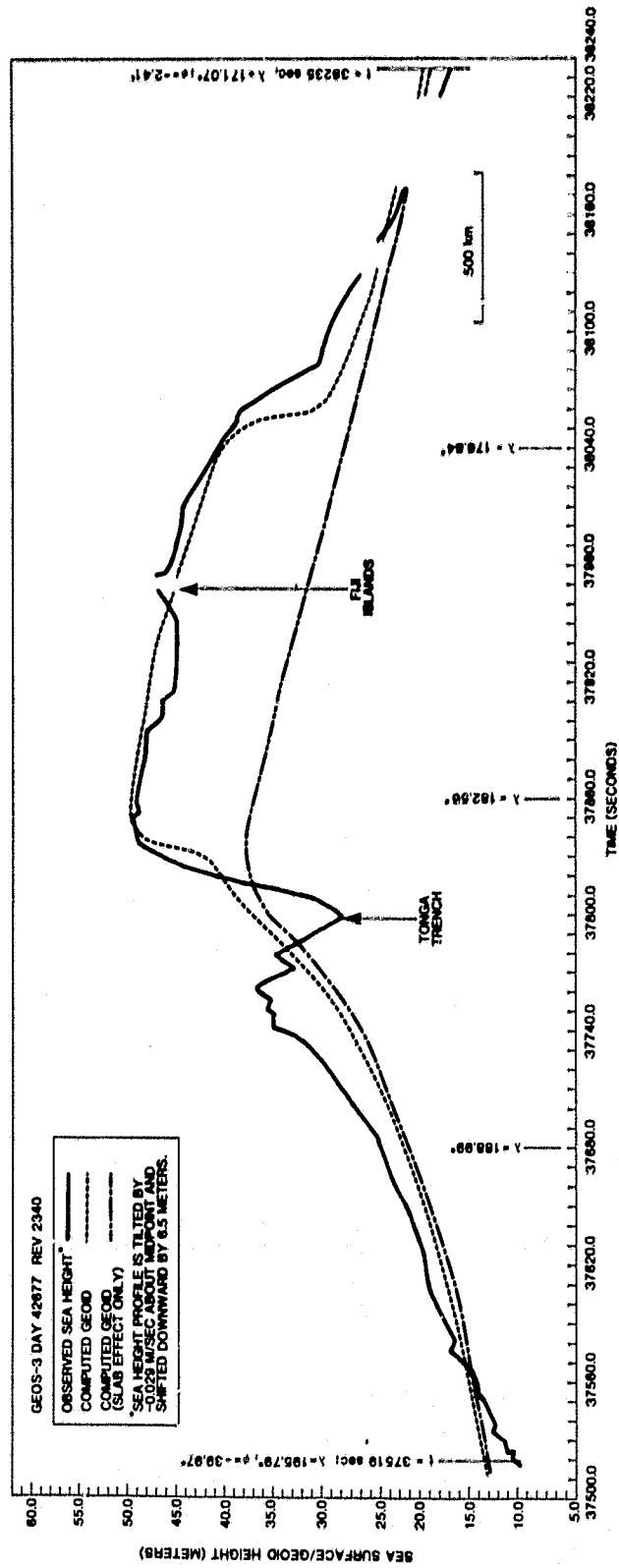Figure 12d. See Figure caption 12a. Sea height profile is from the Geos altimeter.

Figure 12e. See Figure caption 12a. Sea height profile is from the Geos altimeter.

Superposed on this slab effect was the effect due to age variation in the thermal lithosphere (marginal basin effect); this was computed using the very same model that was detailed in the preceding section (see Figure 7).

The agreement in Figures 12a-12e between computed and observed geoids is somewhat rough. However, in light of the major simplifying assumptions, a better agreement can hardly be expected. To obtain a good agreement the observed height profiles have been shifted downward by amounts from 4 to 10 meters. The need for this shift could be ascribed to a number of things including: (i) compensation for orbit or altimeter bias error; (ii) unmodelled gravitational effects of very long wavelength; and (iii) compensation for a rather arbitrary choice of reference ellipsoid. A low degree and order background geoid could have been subtracted from the observed geoid. However, as discussed below and above, this is not appropriate insofar as slabs appear to be capable of significant contributions to the very low degree-and-order field. If a hydrostatic (lower flattening) reference ellipsoid had been used, the shift needed to rectify theory and observation would be increased by about 30 to 40 m. Certain misfits can be readily interpreted as unmodelled effects centered in adjacent areas. For example, there is a long-wavelength low ($\sim$-50 m) in the global geoid which is centered to the south of the region of study at a longitude of roughly 180° and a latitude of -70° This low could conceivably be associated with a component of tilt in the regional geoid of the southwest Pacific. In fact, two sea surface profiles, those of Figures 12b and 12e, have been adjusted using a northwestward tilt of about 0.03 m/sec ($\sim$0.004 m/km). These two profiles are both ascending passes (see Figure 9). The other ascending pass, rev. no. 468 in Figure 12a, has not been adjusted and shows a slight tilt misfit with respect to the model result.

As indicated above, there are areas (marginal basins) which lack sufficient age data to conduct modelling of the effects of the local thermal lithosphere. This explains some of the misfit in the right halves of Figures 12c and 12d.

A summary of slab density anomalies which provide an acceptable fit to observations is given in Table 2. The range (2.6 to 3.2 $\times 10^5$ gm cm^{-2}) in the New Hebrides slab density determination, is due to poorly constrained choice of density for the adjacent NG-NB-S slab complex. As indicated earlier, the 2.6 $\times 10^5$ gm cm^{-2} density is slightly preferred.

DISCUSSION

This study has focused on interpreting a regional marine geoid of the southwest Pacific. There are some clear advantages to applying this same approach to a more global geoid. Estimates of slab density anomalies in this region, or any other individual region, should be somewhat improved by studying the entire marine geoid. Furthermore, a reasonable estimate of the global slab complex's contribution to the geopotential power spectrum could be obtained. Recall that it was shown previously that slabs may, quite conceivably, contribute substantial power for degrees as low as 4 and as high as 20 or greater.

Table 2
Slab Density Determination

SLAB	NOMINAL DENSITY ANOMALY
Tonga-Kermadec	1.0 $\times 10^5$ gm cm^{-2}
New Hebrides	*2.6 $\times 10^5$ gm cm^{-2} **3.2 $\times 10^5$ gm cm^{-2}

*Adjacent NG-NB-S slabs lumped with New Hebrides in assigning densities.
**NG-NB-S slabs lumped with Tonga-Kermadec.

36

As a test of this notion, a geoid was computed from a subset of GEM-9 gravity model coefficients (Lerch et al, 1979) which consisted only of coefficients of degree and order 5 and below. This smoothed geoid retains most of the prominent 73 m high which is centered over New Guinea in the GEM-9 geoid map. The southeastern portion of this high was figured prominently in this study. In fact, this study indicates that a substantial portion of this high is due to dense slabs coupled with beind-arc elevation of the geotherm.

It was also indicated previously that the New Hebrides slab density anomaly (Table 2) may not be typical of slabs worldwide. The nominal density anomaly of the Tonga-Kermadec slab is substantially less (see Table 2). The South-Sandwich slab appears to have a density anomaly of no greater than 1.5×10^5 gm cm^{-2}; this estimate is obtained from a slab model fit to Benioff zone determination of Forsyth (1975) and Brett (1977). If the New Hebrides slab's (and perhaps the NG-NB-S slabs') nominal density anomaly is indeed quite high with respect to most other slabs, then the slabs are not very substantial contributors to the global geopotential spectrum (degree < 20). This remains to be resolved. In any case, there obviously are important large scale gravity anomalies which are not associated with subduction zone density anomalies (see e.g., Cochran and Talwani, 1977, 1978 or McKenzie, 1977).

Adopting the uniform density estimates of 3.2×10^5 gm cm^{-2} one finds that the undetached portion of the New Hebrides slab possesses an inferred negative buoyancy per unit length along strike of 1.1×10^{16} dyne cm^{-1}. Using 1.0×10^5 gm cm^{-2}, one obtains a corresponding buoyancy of 1.0×10^{16} dyne cm^{-1} for the Tonga-Kermadec slab. Using the thermal model due to Molnar and Gray (1979) and McKenzie (1969), theoretical buoyancies of 1.2×10^{16} and 2.8×10^{16} dyne cm^{-1} are obtained for the New Hebrides and Tonga-Kermadec slabs respectively. It appears that the

37

Tonga-Kermadec slab may be regionally compensated (cf. Griggs, 1972) to a large extent whereas the New Hebrides slab may not be. Recall that the New Hebrides slab has an exceptionally high sinking rate (convergence rate ~ 11 cm/yr according to Falvey, 1975; dip exceeds 60°). In estimating buoyancies from the thermal model, plate thicknesses of 100 km (Tonga) and 80 km (New Hebrides) were employed; thermal and physical parameters were taken from Molnar and Gray (1979).

CONCLUSIONS

Undulations in the altimetrically-observed geoid of the southwest Pacific are strongly controlled by (i) positive density anomalies in the subducting slabs of the region (see Table 2) and (ii) the effects of elevation of the geotherm in behind-arc lithosphere (corresponding to young marginal basins). Finer details of slab geometry do not obviously manifest themselves in the observed geoid; such gravitational effects are quite attenuated at sea level and are apparently mixed with crustal effects, oceanographic noise, etc. It appears that slabs in global composite may contribute substantially to intermediate and long wavelength portions (down to spherical harmonic degree 3 or 4) of the earth's gravity field.

ACKNOWLEDGMENTS

REFERENCES

Barazangi, M., B. L. Isacks, J. Oliver, J. DuBois, and G. Pascal, 1973, "Descent of the Lithosphere Beneath New Hebrides, Tonga-Fiji and New Zealand: Evidence for Detached Slabs," Nature, 242, pp. 98-101.

Barnett, C. T., 1976, "Theoretical Modeling of the Magnetic and Gravitational Field of an Arbitrarily Shaped Three-Dimensional Body," Geophysics, 41, pp. 1353-1364.

Billington, S., 1979, "Morphology and Tectonics of the Subducted Lithosphere in the Tonga-Kermadec Region from Seismicity and Focal Mechanism Solutions," Ph.D. thesis, Cornell University.

Brett, C. P., 1977, "Seismicity of the South Sandwich Islands Region," Geophs. J. R. Astr. Soc., 51, pp. 453-464.

Chapman, M. E., 1979, "Techniques for Interpretation of Geoid Anomalies," J. Geophys. Res., 84, pp. 3793-3801.

Chapman, M. E. and M. Talwani, 1979, "Comparison of Gravimetric Geoids with Geos-3 Altimetric Geoid," J. Geophys. Res., 84, pp. 3803-3816.

Chase, C. G., 1979, Subduction, the Geoid, and Lower Mantle Convection, Nature, 282, pp. 464-468.

Chase, C. G., 1971, "Tectonic History of the Fiji Plateau," Bull. Geol. Soc. Amer., 82, pp. 3087-3110.

Cherkis, N. Z., A. Malahoff and J. M. Brozena, 1978, "Magnetic Lineations over the Fiji Plateau," EOS Trans. AGU, 59, p. 266.

Cochran, J. R. and M. Talwani, 1978, "Gravity Anomalies, Regional Elevation and the Deep Structure of the North Atlantic," J. Geophys. Res., 83, pp. 4907-4924.

Cochran, J. R. and M. Talwani, 1977, "Free-Air Gravity Anomalies in the World's Oceans and Their Relationship to Residual Elevation," Geophys. J. R. Astr. Soc., 50, pp. 495-552.

Davis, E. E. and C. R. B. Lister, 1974, "Fundamentals of Ridge Crest Topography," Earth Planet. Sci. Lett., 21, pp. 405-413.

Falvey, D., 1975, Arc Reversals and a Tectonic Model for the North Fiji Basin, Bull. Aust. Soc. Explor. Geophys., 6, pp. 47-49.

Forsyth, D. W., 1975, "Fault Plane Solutions and Tectonics of the South Atlantic and Scotia Sea," J. Geophys. Res., 80, pp. 1429-1443.

Griggs, D. T., 1972, "The Sinking Lithosphere and the Focal Mechanisms of Deep Earthquakes," in The Nature of the Solid Earth, E. C. Robertson (editor), McGraw-Hill, New York, pp. 361-384.

Grow, J. A. and C. Bowin, 1975, Evidence for High Density Crust and Mantle Beneath the Chile Trench due to the Descending Lithosphere, J. Geophys. Res., 80, pp. 1449-1458.

Hamilton, R. M. and A. W. Gale, 1968, Seismicity and the Structure of North Island, New Zealand, J. Geophys. Res., 73, pp. 3859-3876.

Haxby, W. F., 1980, Geoid Anomalies Across Mid-ocean Ridges: A New Constraint on Lithospheric Thermal Models, Earth Planet. Sci. Lett., in press.

Haxby, W. F. and D. L. Turcotte, 1978, On Isostatic Geoid Anomalies, J. Geophys. Res., 83, pp. 5473-5478.

Heiskanen, W. A. and H. Moritz, 1967, Physical Geodesy, W. H. Freeman & Co., San Francisco, p. 97.

Isacks, B. L. and M. Barazangi, 1977, Geometry of Benioff Zones: "Lateral Segmentation and Downwards Bending of the Subducted Lithosphere," Island Arcs, Deep Sea Trenches and Back-Arc Basins, Maurice Ewing Ser., 1, pp. 99-114, AGU, Washington, D.C.

Johnson, T. and P. Molnar, 1972, "Focal Mechanisms and Plate Tectonics of the Southwest Pacific, J. Geophys. Res.," 77, pp. 5000-5031.

Karig, D. E., 1971, "Origin and Development of Marginal Basins in the Western Pacific," J. Geophys. Res., 76, pp. 2542-2561.

Karig, D. E., R. N. Anderson and L. D. Bibee, 1978, "Characteristics of Back Arc Spreading in the Mariana Trough," J. Geophys. Res., 83, pp. 1213-1226.

Kaula, W. M., 1972, "Global Gravity and Tectonics," The Nature of the Solid Earth, E. C. Robertson (editor), pp. 385-405, McGraw-Hill, New York.

Kaula, W. M., 1968, An Introduction to Planetary Physics, John Wiley, New York.

Lambeck, K., 1976, "Lateral Density Anomalies in the Upper Mantle," J. Geophys. Res., 81,

pp. 6333-6340.

Lerch, F. J., S. M. Klosko, R. E. Laubscher and C. A. Wagner, 1979, "Gravity Model Improvement

Using Geos-3 (GEM-9 and -10)," J. Geophys. Res., 84, pp. 3897-3916.

Marsh, J. G., 1980, Unpublished map.

McKenzie, D. P., 1969, "Speculations on the Consequences and Causes of Plate Motions," Geophys.

J. R. Astr. Soc., 18, pp. 1-32.

McKenzie, D. P., 1977, "Surface Deformation, Gravity Anomalies and Convection," Geophys. J. R.

Astr. Soc., 48, pp. 211-238.

Minear, J. W. and M. N. Toksoz, 1970, "Thermal Regime of a Downgoing Slab and New Global

Tectonics," J. Geophys. Res., pp. 1397-1418.

Molnar, P. and D. Gray, 1979, "Subduction of Continental Lithosphere: Some Constraints and

Uncertainties," Geology, 7, No. 1, pp. 58-62.

Morrison, F., 1980, "Computing the Potential and Attraction of a Density Layer by Means of

Elliptic Integrals," Manuscripta Geodaetica, in press.

Parsons, B. and J. G. Sclater, 1977, "An Analysis of the Variation of Ocean Floor Bathymetry and

Heat Flow with Age," J. Geophys. Res., 82, pp. 803-827;

Pascal, G., 1979, "Seismotectonics of the Papua-New Guinea — Solomon Islands Region,"

Tectonophysics, 57, pp. 7-34.

Pascal, G., B. Isacks, M. Barazangi and J. DuBois, 1978, "Precise Relocations of Earthquakes and Seismotectonics of the New Hebrides Island Arc," J. Geophys. Res., 83, pp. 4957-4973.

Paul, M. K., 1974, "The Gravity Effect of a Homogeneous Polyhedron for Three-Dimensional Interpretation," Pure and Appl. Geophys., 112, pp. 553-561.

Pollack, H. N., 1973, "Spherical Harmonic Representation of the Gravitational Potential of a Point Mass, a Spherical Cap and a Spherical Rectangle," J. Geophys. Res., 78, pp. 1760-1768.

Schubert, G., D. A. Yuen and D. L. Turcotte, 1975, "Role of Phase Transitions in a Dynamic Mantle," Geophys. J. R. Astr. Soc., 42, pp. 705-735.

Segawa, J. and Y. Tomoda, 1976, "Gravity Measurements Near Japan and Study of the Upper Mantle Beneath the Oceanic-Trench Marginal Sea Transition Zones," The Geophysics of the Pacific Ocean Basin and Its Margin, Geophysical Monograph 19, G. H. Sutton, M. H. Manghnani and R. Moberly (editors), AGU, Washington, D.C.

Toksoz, M. N. and P. Bird, 1977, Formation and Evolution of Marginal Basins and Continental Plateaus," Island Arcs, Deep Sea Trenches and Back-Arc Basins, Maurice Ewing Ser., 1, pp. 379-393, AGU, Washington, D.C.

Toksoz, M. N., J. W. Minear and B. R. Julian, 1971, Temperature Field and Geophysical Effects of a Downgoing Slab, J. Geophys. Res., 76, pp. 1113-1138.

Turcotte, D. L. and D. C. McAdoo, 1979, "Geoid Anomalies and the Thickness of the Lithosphere," J. Geophys. Res., 84, pp. 2381-2387.

Watts, A. B. and M. Talwani, 1975, "Gravity Effect of Downgoing Lithospheric Slabs Behind Island Arcs," <u>Bull. Geol. Soc. Amer.</u>, 86, pp. 1-4.

Watts, A. B. and J. K. Weissel, 1977, "Tectonic Evolution of the South Fiji Basin," <u>Island Arcs, Deep Sea Trenches and Back-Arc Basins</u>, Maurice Ewing Ser., 1, pp. 419-427, AGU, Washington, D.C.

Weissel, J. K., 1977, "Evolution of the Lau Basin by the Growth of Small Plates," <u>Island Arcs, Deep Sea Trenches and Back-Arc Basins</u>, Maurice Ewing Ser., 1, pp. 429-436, AGU, Washington, D.C.

Weissel, J. K., A. B. Watts, A. Lapouille, G. Karner and D. Jongsma, 1977, "Preliminary Results from Recent Geophysical Investigations in Marginal Basins of Melanesia," <u>EOS Trans. AGU</u>, 58, p. 504.